Review Article

Mohammad Qutob, Mohd Rafatullah*, Mohammad Qamar, Hajer S. Alorfi, Abeer N. Al-Romaizan, and Mahmoud A. Hussein

A review on heterogeneous oxidation of acetaminophen based on micro and nanoparticles catalyzed by different activators

https://doi.org/10.1515/ntrev-2022-0030
received September 28, 2021; accepted January 1, 2022

Abstract: Emerging contaminants are the contaminants that newly identified their adverse effects on the environment. Pharmaceutical compounds have gained researchers' attention among developing organic pollutants as the demand for pharmaceutical compounds has increased, implying their continuing release into the environment. Acetaminophen (ACT) is a popular drug that is wildly used without prescription for the relief of headaches and rheumatic pains. In some places, the detected values of ACT are more than the natural values, which may seriously threaten the environment. Many methods have been applied to remove ACT from water. The advanced oxidation process (AOP) based on micro and nanoparticles has shown promising results to remove ACT from an aqueous medium. This review provides a summary and an organization of the scattered available information related to studies that investigated the removal of ACT from water by an AOP based on micro and nanoparticles. Many topics investigated in this review include the influence of temperature, pH, catalyst concentration, pollutant concentration, the effects of scavengers and oxidants, the stability of the catalyst, and doping ratio. The main results obtained for the removal of ACT by using micro and nanoparticles have been discussed in this review.

Keywords: advanced oxidation process, acetaminophen, paracetamol, heterogeneous, microparticles, nanoparticles

*** Corresponding author: Mohd Rafatullah,** Division of Environmental Technology, School of Industrial Technology, Universiti Sains Malaysia, 11800 Penang, Malaysia, e-mail: mrafatullah@usm.my, mohd_rafatullah@yahoo.co.in, tel: +60-46532111; fax: +60-4656375
Mohammad Qutob: Division of Environmental Technology, School of Industrial Technology, Universiti Sains Malaysia, 11800 Penang, Malaysia
Mohammad Qamar: Interdisciplinary Research Center for Hydrogen and Energy Storage, King Fahd University of Petroleum and Minerals, Dhahran 31261, Saudi Arabia
Hajer S. Alorfi, Abeer N. Al-Romaizan: Chemistry Department, Faculty of Science, King Abdulaziz University, P.O. Box 80203, Jeddah 21589, Saudi Arabia
Mahmoud A. Hussein: Chemistry Department, Faculty of Science, King Abdulaziz University, P.O. Box 80203, Jeddah 21589, Saudi Arabia; Chemistry Department, Faculty of Science, Assiut University, Assiut 71516, Egypt

Abbreviations

ACT	acetaminophen
AO	ammonium oxalate
AOP	advanced oxidation process
BQ	benzoquinone
CF NPs	cobalt ferrite magnetic nanoparticles
CNT	carbon nanotube
CoAl-LDH	CoAl-layered double hydroxide
CS-Fe	chitosan-Fe
CWAO	catalytic wet peroxide oxidation
DO	dissolved oxygen
ECDs	endocrine disrupting compounds
EDTA-2Na	ethylenediaminetetracetic acid disodium
EOCs	emerging organic contaminants
EtOH	ethanol
EPR	electron paramagnetic resonance
Fe/N-CNT	Fe and N codoped carbon nanotube
GAC	granular activated carbon
GR	green rust
IPA	isopropanol
L-his	L-histidine
MCM	mobil composition of matter
MGM	Fe_2O_3
MGN	nanostructured magnetite Fe_2O_3 powders
MnCN	Mn-doped graphite phase carbon nitride
MNPs/β-CDP	magnetite nanoparticles modified β-cyclodextrin crosslinked polymer
MNPs@C	magnetic mesoporous carbon

Mpg-C_3N_4	graphene and mesoporous graphitic carbon nitride
NS-CMK-3	N/S codoped ordered mesoporous carbon
OVPTCN	oxygen vacancies and phosphorus codoped black titania-coated carbon nanotube composites
PAA	application of peracetic acid
PDS	sodium persulfate
PILC	pillared clays
PMS	peroxymonosulfate
POD	horseradish peroxidase
PS	persulfate
PPCPs	pharmaceutical and personal care products
PSW	powdered stone waste
rGO	reduced graphene oxide
SBA-15	Santa Barbara amorphous 15
SOD	superoxide dismutase
TBA	tert butyl alcohol
TCuO50-GO	tomato skin inspired copper oxide-graphene oxide
TEMPOL	4-hydroxy-2,2,6,6-tetramethylpiperidine-1-oxyl
TEOA	triethanolamine
TFSZ	titania loaded fibrous silica
TiO_2 NT	titanium dioxide nanotube
US	ultrasound
UV	ultraviolet light
UVA	ultraviolet with wavelength between 315 and 400 nm
UVC	ultraviolet with wavelength between 100 and 280 nm
WWTPs	wastewater treatment plants
ZIF-8	zeolitic imidazolate frameworks-8
ZSM-5	zeolite socony mobil-5
ZVC	zero-valent copper
ZVI	zero-valent iron

1 Introduction

Emerging organic contaminants (EOCs) have recently gained attention due to their resistance to oxidation and negative impact on the environment [1]. EOCs groups including pharmaceuticals and personal care products, pesticide, disinfection byproducts, wood preservation, endocrine disrupting compounds, bacteria, cyanotoxins, and industrial chemicals [2]. The continuous introduction of these bioactivity compounds into the environment in many ways. Even in low concentrations, they attracted the regulatory organization and governments [3]. Among EOCs compounds, pharmaceutical compounds have attracted real attention because of their negative impacts on public health and the environment [4,5]. Many pharmaceutical products are widely used as anti-inflammatories, analgesic, lipid regulators, antibiotics, antiepileptics, antiseptics, and disinfections. Nowadays, a large number of prescription and nonprescription cure have been used around the world [6–8]. Recently, the consumption of pharmaceutical compounds has increased, which means the continuous release of them into the environment. In the European Union, the use of pharmaceutical compounds could reach thousands of tons per year [9]. With passing time, they may reach a specific concentration causing chronic toxicity effects for humans and the organisms. Moreover, pharmaceutical compounds may enter into the human body through inhalation, ingestion, or transdermal delivery leading to accumulation in tissues, reproductive damage, inhibition of cell proliferation, and behavioral changes [10–12]. It should be noted that there is no standard set for the discharge limits of the pharmaceuticals in an aqueous medium, and the researches that examined pharmaceutical concentrations in water are limited [13]. The sources of pharmaceutical compounds are varied: they could be released from wastewater treatment plants (WWTPs), hospitals, medical care centers, landfills, domestic sewage systems (the drugs could discharge with the urine and manure of the human body through the sewer system), and industries (unused, expired, and residual); as a result, pharmaceutical compounds have been found in the surface water and groundwater [14,15].

Acetaminophen (ACT) or paracetamol ($C_8H_9NO_2$, M_w = 151.163, *N*-(4 hydroxyphenyl)ethanamide) is a popular drug that is widely used without prescription for the relief of headache, migraine, neuralgia, backache, and rheumatic pains [16,17]. The natural value of ACT in the surface water and municipal WWTPs has been detected to be less than 100 ng/L. However, the detected values of ACT in the industrial effluent from a few to tens of milligrams per liter, which may seriously threaten the aquatic organisms and the environment [18–20]. In addition, ACT has some toxic byproducts, such as 1,4-benzoquione and *N*-acetyl-*P*-benzoquinone, which can harm the kidney and liver in humans [21]. Freshwater scarcity, and the rising drinking water demand, is considered one of the environmental problems in the twenty-first century according to its effect on environment, economic, and society [22]. The increase in drinking water demand may attribute to many reasons, such as industrialization, the increase in population, environmental change, and environmental demand. To fulfill the increasing demand for drinking water and to skip any further

accumulation of pollutants in the environment, it has become important to treat contaminated water, and also it helps to remove the pollutants mixing with clean water sources [23]. Many approaches have been applied to remove ACT from water [24–27]. Thus, approaches are classified into three major processes: physical, chemical, and biological process. Among these approaches, chemical oxidation proved its ability to degrade recalcitrant compounds, such as ACT, that resist the bioremediation [18]. The researchers' concern for the ACT degradation is evident from the number of research publications on ACT removal per year, as shown in Figure 1. Last 50 year survey on oxidation of ACT showed 1,620 documents in scopus.com, out of which 56% (900) publications were reported in the last 10 years. Data analysis on the literature survey showed that 92.2% research articles, 4.3% review articles, and 1.6% conference articles were published during this period. This current study, aims to review the recent studies that deal with advanced oxidation process (AOP) based on micro and nanoparticles to remove ACT from an aqueous medium. Also, this study provides a summary and an organization of the scattered available information related to this subject. Many topics investigated in this review include the influence of temperature, pH, catalyst concentration, pollutant concentration, the effects of additives (scavengers and oxidants), the reusability and durability of the catalyst, and doping ratio. The main results obtained for the removal of ACT by using micro and nanoparticles have been discussed in this review.

2 AOP

The mechanism of AOP relies on the activation of some molecules to create reactive species called radicals. The examples of AOP techniques are varied such as Fenton, metal/PS, electrochemical, ultrasound/oxidant, ultrasonic irradiation, ozonation in the presence of particles, and nanoparticles/ultraviolet light (UV). Application of these processes into the water medium generates radicals with a high oxidation–reduction potential that can oxidize different organic compounds [28–31]. There are two mechanisms for the AOP: heterogeneous and homogeneous. In the microcomposite-based and nanocomposite-based catalyst systems, oxidation mainly occurs on the catalyst surface; therefore, the heterogeneous reaction pathway is dominant. Many heterogeneous mechanisms were proposed, for example, singlet oxygen, surface-activated complex, surface-confined sulfate radicals, and surface electron transfer (catalysts as an electron conductor) [32]. Chemical Eqs. (1)–(3) represent iron oxide-based catalyst for heterogeneous nonradical-based reaction and Eqs. (4)–(12) represent iron oxide-based catalyst and persulfate (PS) as an oxidant for homogeneous radical-based reaction [5].

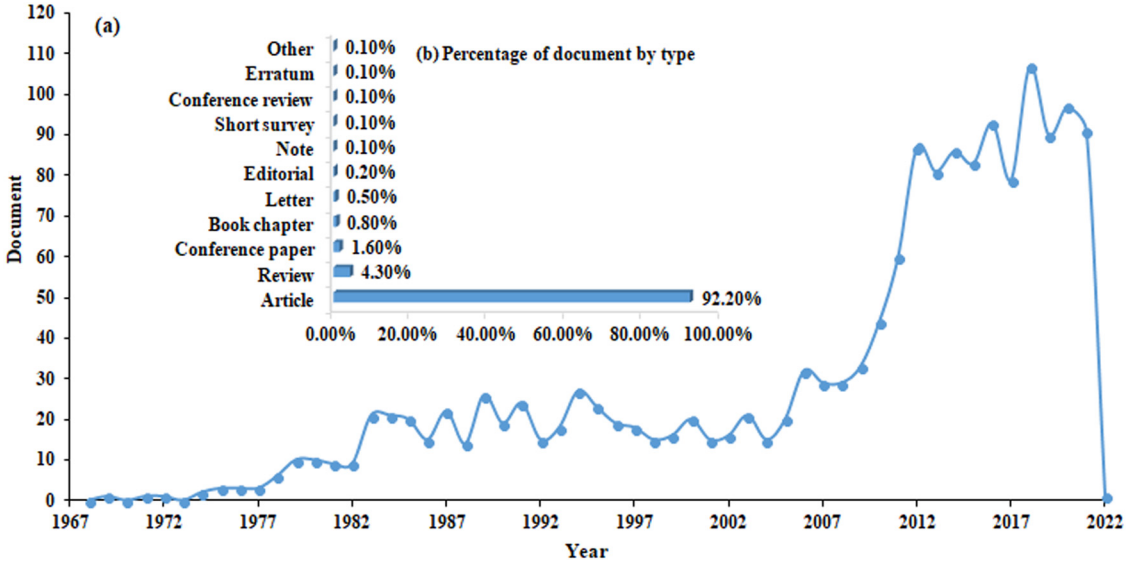

Figure 1: (a) The number of documents of ACT degradation by year and (b) the percentage of each type of documents. Source: Scopus database.

$$\equiv Fe(II) + S_2O_8^{2-} \rightarrow \equiv Fe(III) + SO_4^{\cdot -} \quad (1)$$

$$\equiv Fe(III) + S_2O_8^{2-} \rightarrow \equiv Fe(II) + S_2O_8^{\cdot -} \quad (2)$$

$$\equiv Fe(II) + SO_4^{\cdot -} \rightarrow \equiv Fe(III) + SO_4^{2-} \quad (3)$$

$$SO_4^{\cdot -} + H_2O \rightarrow SO_4^{2-} + H^+ + OH^{\cdot} \quad (4)$$

$$SO_4^{\cdot -} + S_2O_8^{2-} \rightarrow SO_4^{2-} + S_2O_8^{\cdot -} \quad (5)$$

$$OH^{\cdot} + S_2O_8^{\cdot -} \rightarrow HSO_4^- + SO_4^{\cdot -} + \frac{1}{2}O_2 \quad (6)$$

$$OH^{\cdot} + S_2O_8^{2-} \rightarrow OH^- + S_2O_8^{\cdot -} \quad (7)$$

$$SO_4^{\cdot -} + OH^- \rightarrow SO_4^{2-} + OH^{\cdot} \quad (8)$$

$$SO_4^{\cdot -} + SO_4^{\cdot -} \rightarrow S_2O_8^{2-} \quad (9)$$

$$SO_4^{\cdot -} + OH^{\cdot} \rightarrow HSO_5^- \quad (10)$$

$$SO_4^{\cdot -} + \text{Pollutant} \rightarrow \text{Byproducts} \quad (11)$$

$$OH^{\cdot} + \text{Pollutant} \rightarrow \text{Byproducts} \quad (12)$$

A wide variety of AOP systems, including homogeneous and heterogeneous mechanisms, have been applied to degrade ACT from an aqueous medium. AOP systems that are based on homogeneous mechanisms have many drawbacks detected, such as the difficulty of catalyst recovery and metal ions leaching in the reaction media, which caused secondary water pollution [33]. As revealed, heterogeneous catalytic systems such as AOP based on micro and nanomaterials have shown promising results to remove ACT from water [34]. Many semiconductors, such as WO_3, ZnO, SnO_2, TiO_2, CeO_2, Bi_2O_3, and C_3N_4, and metals, such as Fe_3O_2, Fe_2O_3, Al_2O_3, zero-valent aluminum, and Cu_2O, have been used as heterogeneous catalysts. Also, the doping between semiconductors and metals has attracted the researcher's attention according to their advantages, such as reduction in the bandgap of the semiconductors, increase in the bandwidth of absorbance light of the semiconductor surface, and reusability of the composites many times after regeneration.

3 The degradation mechanism of ACT by nanoparticles

The oxidation of ACT based on semiconductors and metal nanomaterials has been gaining the attention because of its high degradation performance, low toxicity, low cost, and ability to function under different conditions. A wide range of activators have been used to catalyze the nanoparticles, such as ultrasound, irradiation (UV and visible light), plasma, and oxidants. The oxidation mechanisms for ACT degradation were varied. Most of the studies observed that the main degradation mechanism was based on the formation of superoxide radicals.

3.1 Mechanism by nanoparticles catalyzed by UV and visible light

Semiconductor nanoparticles capable to generate a hole (h^+) and electrons (e^-) after illuminated with UV or visible light make it the most promising oxidation process as electrons act as reduction agents, whereas holes act as oxidation sites [2]. The mechanism of semiconductors that catalyzed by irradiation, based on photoexcited of the electrons that exist on the catalyst surface, leading to the movement of electrons (e^-) from valance band to conduction band leaving positives holes (h^+). Both electrons and holes can start the redox reactions and oxidize ACT. The mechanism of nanoparticles catalyzed by UV and visible light is depicted in Figure 2.

The equations (13)–(18) represent the possible chemical reactions of TiO_2 catalyzed by UV or visible light system [35].

$$\equiv TiO_2 + hv \rightarrow e_{cb}^- + h_{vb}^+ \quad (13)$$

$$H^- + e^- \rightarrow \text{recombination} \quad (14)$$

$$h_{vb}^+ + H_2O \rightarrow OH^{\cdot} + H^+ \quad (15)$$

$$h_{vb}^+ + OH^- \rightarrow OH^{\cdot} \quad (16)$$

$$ACT + h^+ \rightarrow \text{direct oxidation} \quad (17)$$

$$OH^{\cdot} + ACT \rightarrow \text{direct oxidation} \quad (18)$$

Some disadvantages have been observed related to photodegradation in the presence of semiconductor TiO_2. For example, the high rate of recombination of electrons–holes leading to minimize the degradation of ACT, a wide bandgap of TiO_2, low ionic and electrical conductivity, slow charge transfer rate limits the quantum efficiency of TiO_2 in the photocatalytic reactions, limited adsorption capacity and porosity, and lower efficiency under solar irradiation restricts the application of this system. To decrease the bandgap and enhance the absorption of irradiation of surface catalyst, the researchers have doped semiconductors with transition metals (Co, Fe, Ni, Ag, Au, Cu, Mg, Pt, Zn, Si, and Al) and nonmetals (N and Cl) [17,36–43]. Kohantorabi *et al.* [38] revealed that ACT was completely degraded after 15 min of reaction, and the mineralization was 63% within 1 h when 1.0% w/w Ag/ZnO@$NiFe_2O_4$/PMS/UVA was applied. In addition, Yang *et al.* [44] examined TiO_2 nanoparticles activated by UVC to degrade ACT from a liquid

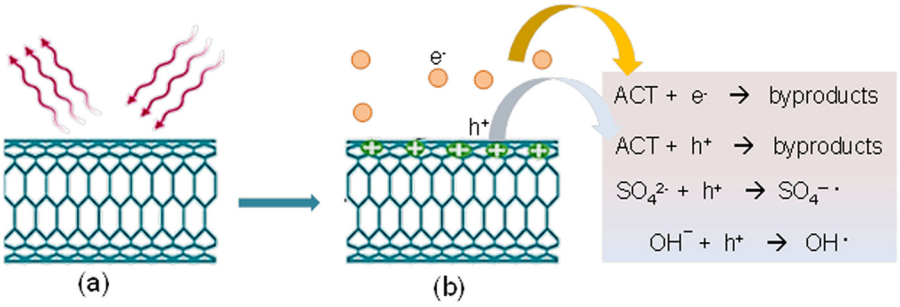

Figure 2: (a) The reaction between irradiation waves and the surface catalyst and (b) reaction leading to the movement of electrons (e^-) from valance band to conduction band leaving positives holes (h^+), which may react directly with ACT as shown in equation (17).

medium. In this system, the initial concentration of ACT was 2.0 mM, and the catalyst concentration was 0.4 g/L. The degradation of ACT was 96% after 80 min of reaction at a pH range of 5.1–3.2. Moreover, Montenegro-Ayo *et al.* [45] applied TiO_2 nanoparticles/UV/0.02 M Na_2SO_4 system to oxidize ACT. Around 72% of ACT was degraded after 300 min. Sun *et al.* [46] applied 0.5 mM N/S codoped ordered mesoporous carbon to catalyze peroxymonosulfate (PMS) for ACT degradation. Around 50 mg/L of ACT was totally oxidized within 30 min, and the mineralization was 27%. The kinetic reaction of ACT in this system was 2.4×10^{-1}/min. Wang *et al.* [47] examined BiOCl/UV/Persulfate system to oxidize ACT from an aqueous medium. The results showed that 50 µM of ACT was completely degraded within 150 min, and the mineralization was 83% after 180 min at pH = 5.4. The kinetic reaction was 7.13×10^{-4}/min. The studies that applied semiconductor as a catalyst and activated by UVA or UVC to degrade ACT from an aqueous medium have summarized in Table 1.

As the catalyzing of nanoparticles by using UV is costly, to avoid that, the researchers intensified on an alternative photocatalytic method such as visible light. As mentioned, TiO_2 powder has a limited absorption capacity of solar light: just around 5% could be absorbed by TiO_2 powder. To enhance the optical absorption of the catalyst, the researchers examined different approaches to improve the TiO_2 performance. Gómez-Avilés *et al.* [2] used C-modified TiO_2 nanoparticles/solar irradiation system for ACT degradation. In this system, ACT was completely removed within 60 min, and the mineralization was 20.4% after 120 min. Da Silva *et al.* [40] studied the degradation of ACT by using 2 g/L of 25% MgO doped with TiO_2 catalyzed by the solar light system. About 48.3% of ACT was degraded within 1 h at pH = 7. Furthermore, Aziz *et al.* [43] applied 5 wt% of TiO_2 doping with SiO_2-ZSM-5/visible light system to remove ACT from an aqueous medium. The results showed around 96% of ACT was oxidized after 180 min, and the mineralization was 77.8%. In addition, 0.1 wt% Cu-doped TiO_2/visible light system was applied by Lin and Yang [48]. The results indicated that 50 mg/L ACT was completely decomposed after 3 h of reaction at pH = 6, and the degradation rate was 0.0243/min. Also, Feng *et al.* [49] examined oxygen vacancies and phosphorus codoped black titania-coated carbon nanotube composites (OVPTCN) activated by a visible light system to degrade and mineralize ACT from a liquid medium. The results were 96 and 20.4% of degradation and mineralization, respectively. Table 2 includes the studies that investigated the semiconductor particles/visible light systems to remove ACT from an aqueous medium.

3.2 Mechanism by nanoparticles catalyzed by oxidants

Many studies investigated the oxidation of ACT by using synthesized particles in the presence of oxidants. For example, Ikhlaq *et al.* [50] examined the oxidation of ACT by zeolite/O_3 system. They proposed that both ACT and O_3 were adsorbed on the surface of zeolite then react with each other, which supports that the nonradical mechanism was dominant. Figure 3 illustrated the adsorption of oxidant and ACT on the catalyst surface, then the oxidant attacked ACT, which resulted in the degradation of the pollutant *via* the heterogeneous or nonradical mechanism.

In addition, heterogeneous and homogeneous could happen together. Mashayekh-Salehi *et al.* [3] applied MgO/O_3 system to oxidize ACT in an aqueous solution. They proposed the following chemical equations (19)–(25) that might happen while the degradation reaction is running.

- Direct oxidation with O_3 molecules on MgO surface:

$$MgO - O_3 + ACT \rightarrow H_2O_2 + CO_2 + \text{Intermediates} \quad (19)$$

Table 1: Summary of studies that investigated semiconductor/UV systems for removal of ACT

Systems	BET surface area (m^2/g)	Particle size (nm)	Pore volume/pore diameter/pore size	pH	Mineralization	Removal	Time (min)	[ACT]	[Catalyst]	Ref.
TiO_2	*	*	*	7.9	59% within 5 h	96%	300	50 ppm	2 g/L	[8]
TiO_2 with flow O_2 (100 mL/min)					72% within 4 h	100%	240			
25% Mg–SiTi	382	*	0.09 cm^3/g, 16.8 nm	4.3	*	60%	60	20 mg/L	0.7 g/L	[40]
TiO_2 with O_2 concentration 34 mg/L	50	21	*	5.1–3.5	60% after 300 min and 85% within 450 min	95%	80	2.0 mM	0.4 g/L	[44]
BiOCl/UVA/PS	20.11	*	0.1005 cm^3/g, 19.98 nm	5.4	83% after 180 min	100%	150	50 µM	0 g/L	[47]
TiO_2	*	*	*	7	*	72.7%	60	0.017 mM	0.3 g/L	[54]
Combination of TiO_2 with graphene oxide TiO_2@rGO TG_3	114.3	20	8.3 nm	5.4	92% of ACT was mineralized within 50 min	100%	50	50 mg/L	2 g/L	[59]
Combination of TiO_2 with graphene oxide TiO_2@rGO TG_5	139		5.4 nm			87%	50			
Combination of TiO_2 with graphene oxide TiO_2@rGO TG_{10}	166.5		2.6 nm			70%	50			
15% TiO_2/Fe_2O_3 core–shell nanostructure	59.32	Nanoparticles	0.165 cm^3/g, 11.12 nm	*	*	64.5%	90	50 mg/L	0.1 g/L	[60]
33% TiO_2/Fe_2O_3 core–shell nanostructure	70.78		0.169 cm^3/g, 9.56 nm		*	75% with flow 100 mL/min of O_2 reached to 99%	90			
50% TiO_2/Fe_2O_3 core–shell nanostructure	125		0.245 cm^3/g, 7.813 nm		With purge 100 mL/min of O_2 TOC 66%	87.8% With purge 100 mL/min of O_2 99%	90			
Anatase TiO_2 hollow sphere fabricated through a template solvothermal route	164	4.0–5.0 nm	0.32 cm^3/g	*	*	94%	60	50 mg/L	0.1 g/L	[61]
ZnO/PSW-contained sono-reactor	12.773	*	2.934 cm^3/g	Natural pH	40% 240 min	98.1%	60	10 mg/L	0.7 g/L	[73]
CNT10	348–421	5–6 nm	0.284 cm^3/g	7	61.2% after 60 min	81.6 ± 0.6%	60	10 mg/L	*	[75]
TiO_2-Rutile	*	*	*	*	*	70%	50 h	1 mM	1 g/L	[76]
TiO_2-Anatase						More than 50%				
TiO_2 80% Anatase, 20% rutile	51–55	30–50	*	Natural pH	11% within 72 min	100%	72	10 mg/L	200 mg/L	[77]
TiO_2/UV in wastewater					21% within 72 min	100%	24			

(*Continued*)

Table 1: *Continued*

Systems	BET surface area (m^2/g)	Particle size (nm)	Pore volume/pore diameter/pore size	pH	Mineralization	Removal	Time (min)	[ACT]	[Catalyst]	Ref.
TiO_2 thin films calcinated at 650°C	*	Nanoparticles	800 nm	*	*	100%	150	1 mg/L	*	[78]
TiO_2 modified with electrolysis/H_2O_2/UV	115.4	9.3 nm	0.2 µm	5.5	26.20%	76%	90	0.1 g/L	0.5 g/L	[79]
Cu/iron-pillared clay/UV	110	*	1.76 cm^3/g, 3.82 nm	2.7–3	80% after 180 min	100%	60	100 mg/L	0.5 g/L	[80]
Sonophotocatalytic/MnO_x-TiO_2	132	181 µm	0.14–0.21 cm^3/g	*	*	26%	180	25 ppm	0.1 g/L	[81]
PAA/UVC-LED/Fe(II)	*	*	*	5	*	95%	30	20 mg/L	(PAA) 4 mM and 0.5 mM Fe(II)	[82]
Photo-Fenton process	*	14 nm	*	3.5	*	85%	*	20 mg/L	0.2 g/L	[83]
Photo-Fenton	*	*	*	2.8	77% after 75 min	100%	15	0.62 mM	0.18 mM	[84]
MNPs@C/UV/PMS	572.6	*	0.379 cm^3/g	6	63.5% after 40 min	97.4%	40	20 mg/L	0.16 g/L	[85]
Photo Fenton-like oxidation process	Between 1 and 6	*	*	Natural pH	*	86.9%	60	10 mg/L	0.1 g/L	[86]
Zeolite-TiO_2	49	*	*	5	*	44.3%	180	20 mg/L	1 g/L	[87]
Zeolite-ZnO	98					58.7%				
3% (w/w) of $WO_3/TiO_2/SiO_2$ composite under UV-VIS irradiation	167.30	*	0.67 cm^3/g	9	*	Higher 95%	240	5 mg/L	1.5 g/L	[88]
Combining ZVI reduction with photo-Fenton	*	*	*	3.5	*	75%	60	5 mg/L	*	[89]
La-doped $BiFeO_3$/rGO	31.79	5–6 nm	7.31 cm^3/g	*	*	98.6%	30	50 ppm	0.2 g	[90]

*Means data not available; BET: Brunauer, Emmett and Teller.

Table 2: Summary of studies that investigated semiconductor particles/visible light systems for the removal of ACT

Catalysts	BET surface area (m^2/g)	Particle size (nm)	Pore volume/pore diameter/pore size	Removal (%)	Time (min)	pH	[ACT]	[Catalyst]	Mineralization	Ref.
C-modified TiO_2 calcinated at 400°C	147	11.8	0.87 cm^3/g	100	60	*	5 mg/L	250 mg/L	*	[2]
C-modified TiO_2 calcinated at 500°C	111	17	0.9 cm^3/g							
25% Mg–SiTi	382	*	0.09 cm^3/g, 16.8 nm	48.3	60	4.3	20 mg/L	0.7 g/L	*	[40]
4% Ag-*g*-C_3N_4/O_3	6.3	*	*	*	*	7, 8, and 9	10 mg/L	0.25 g/L	83% within 120 min	[41]
TiO_2-fibrous silica (0.1 M)	531	*	1.215 cm^3/g	88	180	5	10 mg/L	0.5 g/L	*	[43]
TiO_2-fibrous silica (0.2 M)	525		1.102 cm^3/g	96	180					
TiO_2-fibrous silica (0.3 M)	633		1.309 cm^3/g	67	180					
0.1 wt% Cu-doped TiO_2	120	8.2	5.6 nm	100	180	6	50 mg/L	4 g/L	*	[48]
OVPTCN	104.71 cm^2/g	*	*	96	120	*	5 ppm	0.5 g/L	20.4% after 120 min	[49]
BaTi O_3/TiO_2 (1:3)	*	*	*	95	240	7	5 mg/L	1 g/L	*	[55]
BaTi O_3/TiO_2 (1:1)										
BaTi O_3/TiO_2 (3:1)										
Ag/AgCl at ZIF-8	367.4	*	*	99	90	5	1 mg/L	0.5 g/L	*	[57]
TiO_2 modified with electrolysis/visible light/H_2O_2	115.4	9.3 nm	0.2 µm	60	90	5.5	0.1 g/L	0.5 g/L	20.50% within 90 min	[79]
$K_2S_2O_8$-doped TiO_2	*	*	*	100	540	6.9	0.1 mM	1 g/L	*	[91]
Photo-Fenton using FeO_x	*	*	*	100	180	2.5	0.05 mM	50 mg/L	58% after 300 min	[92]
Photo-Fenton using $FeSO_4$				100	120				79% after 300 min	
β-Bi_2O_3	*	70	*	93.6	180	*	10 mg/L	50 mg	89.5% after 240 min	[93]
Photo-Fenton solar process/synthesized wastewater	*	*	*	90	36	Neutral pH	1 ppm	3 ppm	26.5%	[94]
Novel siligraphene/*g*-C_3N_4 composites	173.44	*	0.29 cm^3/g	80	20	Less than 6	5 mg/L	0.015 g	*	[95]
UiO-66-NH_2	904	*	0.48 cm^3/g	90	6 h	*	5 mg/L	250 mg/L	*	[96]
Fe_2O_3–TiO_2 nanocomposites by	84	*	0.115 cm^3/g	95.85	180	11	30 mg/L	1.25 g/L	*	[97]

*Means data not available.

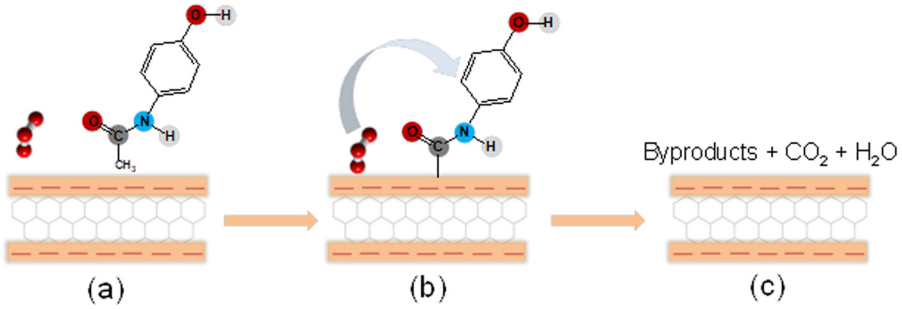

Figure 3: (a) Both ACT and O_3 were adsorbed on the zeolite surface, (b) O_3 was attacked with ACT, and (c) both O_3 and ACT were oxidized.

$$MgO - ACT + O_3 \rightarrow H_2O_2 + CO_2 + Intermediates \quad (20)$$

- Radical type catalytic oxidation on MgO surface:

$$MgO - S + O_3 \rightarrow MgO^{O^{\cdot}} + O_2 \quad (21)$$

$$MgO - S^{O^{\cdot}} + 2(H_2O) + O_3 \rightarrow MgO - S^{OH^{\cdot}} + 3(OH)^{\cdot} + 2O_2 \quad (22)$$

$$MgO - S^{(OH^{\cdot})_2} + ACT \rightarrow H_2O_2 + CO_2 + Intermediates \quad (23)$$

- Direct oxidation with O_3 molecules in the bulk solution:

$$O_3 + ACT \rightarrow H_2O_2 + CO_2 + Intermediates \quad (24)$$

- Radical type catalytic oxidation in the bulk solution:

$$OH^{\cdot} + ACT \rightarrow H_2O_2 + CO_2 + Intermediates \quad (25)$$

The symbol S in the Eqs. (21)–(23) represents Lewis acid sites on the surface of MgO composites, which were available for reacting with ozone. Hydrogen peroxide (H_2O_2) has been used as an oxidant to promote the degradation of ACT. For example, the doping of bimetallic iron–copper in the presence of $S_2O_8^{2-}$ and H_2O_2 has been applied.

The Eqs. (26)–(31) represent the main chemical equations of generating hydroxyl radicals onto iron and copper oxide surfaces [51]:

$$\equiv Cu^0 + \frac{1}{2}H_2O_2 + Hc^+ \rightarrow \equiv Cu^+ + H_2O \quad (26)$$

$$\equiv Cu^{1+} + H_2O_2 \rightarrow \equiv Cu^{2+} + OH^{\cdot} + OH^- \quad (27)$$

$$\equiv Cu^{2+} + H_2O_2 \rightarrow \equiv Cu^{1+} + HO_2^{\cdot} + H^+ \quad (28)$$

$$\equiv Fe^{2+} + H_2O_2 \rightarrow \equiv Fe^{2+} + OH^{\cdot} + OH^- \quad (29)$$

$$\equiv Fe^{3+} + H_2O_2 \rightarrow \equiv Fe^{2+} + HO_2^{\cdot} + H^+ \quad (30)$$

$$\equiv Fe^{3+} + \equiv Cu^{1+} \rightarrow \equiv Fe^{2+} + \equiv Cu^{2+} \quad (31)$$

The possible reactions in the presence of PS are presented in Eqs. (32)–(36) [52]:

$$\equiv Cu^{1+} + S_2O_8^{2-} \rightarrow \equiv Cu^{2+} + SO_4^{\cdot-} \quad (32)$$

$$\equiv Cu^{2+} + S_2O_8^{2-} \rightarrow \equiv Cu^{3+} + SO_4^{\cdot-} \quad (33)$$

$$\equiv Fe^{2+} + S_2O_8^{2-} \rightarrow \equiv Fe^{3+} + SO_4^{2-} + SO_4^{\cdot-} \quad (34)$$

$$\equiv Fe^{3+} + HSO_5^- \rightarrow \equiv Fe^{2+} + SO_5^{\cdot-} + H^+ \quad (35)$$

$$S_2O_8^{2-} + H_2O \rightarrow HSO_5^- + HSO_4^- \quad (36)$$

The possible reactions Eqs. (37)–(39) in the presence of PMS are as follows [53]:

$$\equiv Fe^{2+} + HSO_5^- \rightarrow \equiv Fe^{2+} - (OH)OSO_3^- + OH^- \quad (37)$$

$$\equiv Fe^{2+} - (OH^-) + HSO_5^- \rightarrow \equiv Fe^{3+} + SO_4^{2-} + OH^{\cdot} \quad (38)$$

$$\equiv Fe^{2+} - (OH)OSO_3^- \rightarrow \equiv Fe^{2+} - (OH^-) + SO_4^{\cdot-} \quad (39)$$

Furthermore, in the systems that relay on PS and PMS as a catalyst, the reaction may go further to produce hydrogen peroxide ($OH^{\cdot}$) as in the following Eqs. (40)–(44) [5].

$$SO_4^{\cdot-} + H_2O \rightarrow SO_4^{2-} + H^+ + OH^{\cdot} \quad (40)$$

$$S_2O_8^{2-} + OH^{\cdot} \rightarrow SO_4^{2-} + S_2O_8^{\cdot-} \quad (41)$$

$$OH^{\cdot} + S_2O_8^{\cdot-} \rightarrow HSO_4^- + SO_4^{\cdot-} + \frac{1}{2}O_2 \quad (42)$$

$$OH^{\cdot} + S_2O_8^{\cdot-} \rightarrow OH^- + S_2O_8^{\cdot-} \quad (43)$$

$$OH^- + SO_4^{\cdot-} \rightarrow SO_4^{2-} + OH^{\cdot} \quad (44)$$

Table 3 lists the studies that applied metals and semiconductor particles catalyzed by oxidants to remove ACT from the aqueous medium.

4 The influence of different parameters on ACT degradation

Many different parameters that influence the degradation of ACT such as temperature, pH, catalyst concentration, pollutant concentration, effects of additives (scavengers

Table 3: Summary of the studies that investigated the removal of ACT by synthesized particles

Catalyst	BET surface area (m^2/g)	Particle size (nm)	Pore volume/and pore diameter/ pore size	Oxidant concentration	Removal (%)	Time (min)	Mineralization	[ACT]	[Catalyst]	pH	Ref.
Pt-supported nanocomposites of Al_2O_3	*	*	*	$[O_3]$ = 3 mg/min	100	9	24% after 60 min	35 µM	5 mg/L	7	[17]
1.0% w/w Ag/ ZnO0.04@$NiFe_2O_4$/UVA	25.01	Nano rod	6.98 cm^3/g	[PMS] = 0.2 mM	100	15	63% after 60 min	12 mg/L	0.1 g/L	7	[38]
$CoFe_2O_4$/mpg-C_3N_4	111.06	14.8	0.69 cm^3/g, 12.49 nm	[PMS] = 1.5 mM	92	25	65% after 60 min	15 mg/L	40 mg/L	7	[39]
N/S codoped ordered mesoporous carbon	545.6	*	2–50 nm	[PMS] = 0.5 mM	100	30	27%	50 mg/L	100 mg/L	3.5–9	[46]
Bismuth oxychloride BiOCl	20.11	*	0.1005 cm^3/g, 19.98 nm	$[Na_2S_2O_8]$ = 1 mM	100	150	More than 85% after 180 min	50 µM	0.3 g/L	5.4	[47]
Zeolite	91.35	*	4 Å	$[O_3]$ = 0.9 mg/min	90.68	60	*	50 mg/L	5 g	7.12	[50]
Fe_3O_4@SiO_2@Cu yolk–shell nanostructures	458.86	*	0.41 cm^3/g	$[H_2O_2]$ = 15 mM	Near 100	20	*	2 mg/L	0.2 g/L	5	[51]
Fe_2O_3 at Cu_2O	*	*	2–2.5 µm	[PS] = 0.6 g/L	90	40	*	100 mg/L	0.3 g/L	6.5	[52]
Fe_3O_4 magnetic nanoparticles	85.2	20	0.302 cm^3/g, 13.8 nm	[PMS] = 0.2 mM	75	120	*	10 mg/L	0.8 g/L	Around 7	[53]
Modified MgO nanoparticles	257.3	23.6	0.22 µm	$[O_3]$ = 1.8 mg/min	94	30	*	50 mg/L	2 g/L	5.4	[56]
Mn Fe_2O_4	*	*	*	[PMS] = 0.2 mM	100	60	3.5% after 120 min	10 mg/L	0.2 g/L	4.3	[58]
Co Fe_2O_4					90.5		16.5% after 120 min				
Fe_2O_3 at Cu_2O	*	*	15 µm	[PS] = 0.8 g/L	92	90	*	100 mg/L	Fe^{2+} = 0.7 mM CuO = 0.3 g/L	6.5	[63]
Pyrite	*	*	*	$[H_2O_2]$ = 5 mM	100	180	*	50 mg/L	2 g/L	4	[64]
Pyrite				[PDS] = 5 mM	96	180					
Green rust SO_4/Cu(II)	*	*	*	*	82	360	*	50 mg/L	[Fe(II)] = 1 g/L	6	[67]
Green rust CO_3/Cu(II)					28						
Green rust Cl/Cu(II)					74				[Cu(II)] = 0.3 g/L		
Zero-valent aluminum	*	*	Micropores	[PS] = 2 mM	98.5	35	*	30 mg/L	2 g/L	7	[65]
Nanostructured magnetite (Fe_3O_4) powders MGN1	39.6	29	*	$[H_2O_2]$ = 153 mM/L	100	300	41% after 6 h	100 mg/L	6 g/L	2.6	[70]
MGN2	5.84	208					34% after 6 h				
MGM	48	35					39% after 6 h				
Fe/N-CNT	*	*	*	[PS] = 0.08 mM	98.4	30	*	10 mg/L	0.05 g/L	2.0–8.2	[74]
Cu/Fe-PILC	110	*	1.76 cm^3/g, 3.82 nm	$[H_2O_2]$ = 483 mg/L	100	60	80% after 180 min	100 mg/L	50 mg/L	2.7	[80]
Iron oxide–silica	734	*	0.95 cm^3/g	$[H_2O_2]$ = 17 mM	80	20–30	*	20 mg/L	0.3 g/L	Natural pH	[98]

(*Continued*)

Table 3: *Continued*

Catalyst	BET surface area (m^2/g)	Particle size (nm)	Pore volume/and pore diameter/ pore size	Oxidant concentration	Removal (%)	Time (min)	Mineralization	[ACT]	[Catalyst]	pH	Ref.
US/Fenton/TiO_2 NT	*	*	*	US1000 kHz	85.3	30	*	3 µM	Fe^{2+}:H_2O_2 ratio of 20:4	3	[99]
Iron ore tailings	74	*	1.2 nm	[H_2O_2] = 6.2 mol/L	100	30	*	2 mg/L	250 mg	7.6	[100]
Zero-valent aluminum under air-equilibrated acidic conditions	*	75–150 µm	*	*	99	960	*	20 mg/L	2 g/L	1.5	[101]
Bicarbonate	*	*	*	[PS] = 5 mM	More than 50	8 h	*	10 µM	25 mM	8.3	[102]
Fenton oxidation system	*	*	*	[H_2O_2] = 15 mM	91.2	60	*	5 mM	0.055 mM	3	[103]
Fenton process system	*	*	*	[H_2O_2] = 13.8 mM	92	30	34% after 60 min	200 ppm	5 mM	3	[104]
Aerated Fenton reactor system	*	*	*	[H_2O_2] = 25 mM	99	40	14% after 40 min	5 mM	0.1 mM	3	[105]
GAC	939.38	*	0.54 cm^3/g	[PS] = 0.21 mM	100	90	*	10 mg/L	1 g/L	3–7	[106]
CNT	201.04		1.91 cm^3/g		100	60			0.1 g/L		
Co-FeOCl	10.39	*	0.073 cm^3/g	[H_2O_2] = 0.5 mM	87.5	60	*	10 µM	0.2 g/L	7	[107]
TCuO50-GO/CWAO	7.74	*	*	*	96.2	60	52.1% after 60 min	100 mg/L	0.5 g/L	5.5	[108]
Fe-SBA-15(20)Fe_2 $(SO_4)_3$	801	*	*	[H_2O_2] = 25 mg/L	90.8	120	64% after 240 min	20 mg/L	1,000 mg/L	4.5	[109]
Fe-SBA-15(20)$FeCl_3$	705				10.5		Less than 2% after 240 min				
MNPs/β-CD	112	*	0.138 cm^3/g	[$KMnO_4$] = 21.7 µM	95.6	10	*	3.31 µM	MNPs/β-CDP 3.33 g/L	Initial 7	[110]
0.5-MnCN	*	*	*	[PMS] = 0.8 g/L	100	15	*	20 mg/L	200 mg/L	6.5	[111]
TiO_2-rGO 5%/plasma	*	*	*	*	92	18	*	20 mg/L	0.25 g/L	9.5	[112]
ZVC	*	*	*	O_2	100	4 h	*	50 mg/L	5 g/L	3	[113]
CoAl-LDH	52.9	*	0.122 cm^3/g	[PMS] = 0.5 mM	97.5	10	*	10 mg/L	0.15 g/L	6	[114]
CoAl-CLDH-300	251.4		0.263 cm^3/g		96.9		60.9% after 4 h				
SnO_2	81	5.5		[O_3] = 1.6 mg/min	98	20	84% after 30 min	50 mg/L	1.3 g/L	7	[115]
Zn/MCM	650	*	0.643 cm^3/g	Stochiometric amount of [H_2O_2]	10	240	*	5 mg/L	1 g/L	3	[116]
Fe/MCM	640		0.738 cm^3/g		100	240					
Cu/MCM	950		0.727 cm^3/g		More than 50	240					
Cr/MCM	780		0.694 cm^3/g		100	60					

*Means data not available.

and oxidants), flow O_2, and doping ratio have been investigated.

4.1 The influence of ACT concentration

Major studies that have applied AOP systems in the presence of synthesized particles for ACT oxidation pointed out that when the ACT concentration increases, the degradation efficiency decreases. For systems based on oxidants such as hydrogen peroxide, PS, and PMS, high ACT concentrations may adsorb and cover a wide number of the active sites on the catalyst's surface, consequently, suppressing the production of super oxidant radicals. Also, for the systems that depend on UV or visible lights as a catalyst, a high ACT concentration may accumulate on the catalyst surface and prevent the penetration of the irradiation, which may reduce the photocatalytic efficiency. For example, Yang *et al.* [44] applied TiO_2 catalyzed by UVA and UVC. They carried out different ACT initial concentrations from 2 to 10 mg/L. The removal decreased from 95% to less than 20%. Montenegro-Ayo *et al.* [45] studied the changes in the degradation rate when the initial concentration of ACT increased from 5 to 50 mg/L. The results showed a decrease in the oxidation rate from 2.05×10^{-4} to 2.86×10^{-5}, respectively. Also, Tan *et al.* [54] examined TiO_2 activated by UV system to eliminate ACT from liquid medium. The oxidation of ACT was declined from 72.7 to 40.2% when the ACT initial concentration increased from 0.017 to 0.067 mM, respectively. Furthermore, Kurniawan *et al.* [55] applied photocatalytic of $BaTiO_3/TiO_2$ composites to remove ACT; 5 and 25 mg/L of initial ACT concentration were implemented, and the results were a decline in the degradation efficiency from 81 to 19%. The same results were observed when Yaghmaeian *et al.* [56] carried out modified MgO nanoparticles catalyzed by ozone. When the initial concentration of ACT was 10, 50, 100, and 200 mg/L, the removal was 99.5, 99.4, 77, and 45%, respectively. However, Fan *et al.* [57] observed that when the initial ACT concentrations were 0.5, 1.0, and 1.5 mg/L at Ag/AgCl@ZIF-8/visible light system, the removal efficiency was stable at 99% after 60 min. They reported that when the concentration was between 0.5 and 1.5, the reaction rate reached the fastest at 1.5 mg/L. However, when the initial concentration exceeds 2.0 mg/L, the reaction rates decrease because the permeability of the photon would reduce when the substrate concentration was too high.

4.2 The influence of semiconductor and metal dosages

Most studies agreed that when the catalyst concentration increases to a certain level, it may benefit and increase the degradation reaction. However, if an excessive amount of catalyst adds, that maybe affected adversely on the degradation performance, or at least the degradation performance stays similar. For systems based on photocatalytic, that might interpret because, at high catalyst concentrations, the agglomeration and the shielding effect of the suspended catalyst is due to increased turbidity and impedes the light penetration, which reduces the accessible light to the catalyst surface resulted decreasing in the photocatalytic. For AOP-nanocomposite systems that based on irradiation activation such as hydrogen peroxide, PMS, and PS, high catalyst concentration leading to an increase in the number of activated radicals, which leads to the self-consumption of generated radicals. Below are some studies that investigated different catalyst concentrations. Hassani *et al.* [39] carried out different concentrations of $CoFe_2O_4$/mpg-C_3N_4 nanoparticles to activate PMS when the catalyst concentration increased from 10 to 40 mg/L, the removal enhanced from 53 to 85% within 25 min. Although the concentration increased from 40 to 60 mg/L, the oxidation was still the same. Zhang *et al.* [52] implemented iron–copper bimetallic/PS system to degrade ACT and observed improvement in the degradation percentage at catalyst concentrations between 0.1 and 0.3 g/L, the removal increased from 38.6 to 90%. When 0.4 g/L of catalyst was added, there was no significant change in the degradation performance. Thus, it might be because the excessive amount of $SO_4^{\cdot-}$ increases the self-consumption as Eq. (45):

$$SO_4^{\cdot-} + SO_4^{\cdot-} \rightarrow S_2O_8^{2-} \quad (45)$$

Furthermore, $MnFe_2O_4$/PMS and $CoFe_2O_4$/PMS systems were applied by Tan *et al.* [58], and the results were 96.7, 100, 100, and 100% for $MnFe_2O_4$/PMS system and 61, 99.5, 100, and 100% for $CoFe_2O_4$/PMS at 0.1, 0.2, 0.3, and 0.4 g/L, respectively. Cheshme Khavar *et al.* [59] mentioned the effect of catalyst dosage when the LED/titanium dioxide doped with graphene oxide (TiO_2@rGO) system was applied to remove ACT. They implemented TiO_2@rGO concentrations from 0.4 to 4 g/L. It observed that when the catalyst concentrations were 0.4, 1, and 2 g/L, the removal was 53, 57, and 81%, respectively. Meanwhile, when the concentration of TiO_2@rGO increased from 2 to 4 g/L, there was no improvement in the degradation

of ACT. Moreover, Abdel-Wahab *et al.* [60] examined the TiO_2/Fe_2O_3/UV system that when the catalyst concentration increased from 0.1 to 2 g/L, the reaction rate was strongly affected, while concentrations between 0.1 and 1.2 g/L, the removal rate increased because the number of active sites and activated radicals increased. Hence, at 2 g/L of TiO_2/Fe_2O_3 was applied, the degradation rate was declined. Also, different $K_2S_2O_8$-doped TiO_2 dosages have been applied. From 0.25 to 0.5 g/L concentration, the oxidation of ACT increased from 90 to 100% after 9 h. When the dosage increases from 0.5 to 1.5 g/L, the removal was kept around 100% and reached the fastest reaction rate at 1 g/L. While at 2 g/L was applied, the degradation dropped from 100 to 97% [61].

4.3 The influence of pH

pH is a significant factor in the AOP based on semiconductors and metal systems. The effect of pH in (AOP/composites) system for the degradation of ACT is widely investigated. It has been observed that ACT has two chemical forms depending on the pH: (i) nonionic form when the pK_a is under 9.4 and (ii) ionic form when pK_a is more than pH 9.4. In addition, pH_{zpc} and the type of composite were the main variables to define the oxidation performance of ACT [62]. For example, Ziylan-Yavaş and Ince [17] studied the degradation of ACT by using Pt-supported nanocomposites of the Al_2O_3/O_3 system. The results showed that at the base and neutral pH conditions, ACT was eliminated in 7 and 10 min, respectively. The carbon mineralization increased when increasing the pH because the consumption of ozone increased with increasing pH. That might be attributed to the increase in O_3 that converted to $OH^{\cdot}$ at high pH atmosphere. The impact of pH between 4 and 10 on the oxidation of ACT by using 1.0% w/w Ag/ZnO0.4@ $NiFe_2O_4$/PMS/UVA system was investigated. The best result was obtained at pH between 6 and 7. Because at this pH, the HSO_5^- ions can be attracted to the positive surface of the catalyst, which improve the oxidation efficiency by the production of $OH^{\cdot}/SO_4^{\cdot-}$. At acidic conditions, the activation of PMS was decreased due to the H-bond formation between H^+ and O–O group of HSO_5, which declines the ACT removal [38]. Hassani *et al.* [39] studied the impact of pH from 3 to 11 on the oxidation of ACT by using the $CoFe_2O_4$/mpg-C_3N_4 system. They revealed that the best result was obtained when the pH was 7. Both acidic and base conditions were not favorable for degradation in this system. In the acid atmosphere, the oxidation of ACT was not good for two reasons because the activation of PMS was decreased due to the H-bond formation between H^+ and O–O group of HSO_5^-, which decreased the ACT removal, and both $SO_4^{\cdot-}$ and $OH^{\cdot}$ react with H^+ resulted in reducing in the degradation of ACT. In alkaline conditions, there were some possible reasons responsible for decreasing ACT degradation: (1) converting $SO_4^{\cdot-}$ radicals to $OH^{\cdot}$ species with relatively lower redox potential by OH^- ions, (2) formation of metal hydroxide complexes of CFNPs and subsequently decrease of PMS decomposition reactions, and (3) self-decomposition of PMS to water and sulfate ions. Ling *et al.* [41] examined the influence of pH on the mineralization of ACT when (solar/4% Ag-*g*-C_3N_4/O_3) system was implemented. They applied the following pH: 3, 5, 7, 9, and 11. From pH 3–7, the degradation of ACT was enhanced because the increase of pH value increases the conversion of O_3 to $OH^{\cdot}$, which degrades more ACT effectively when the pH increased from 7 to 11, the removal of ACT kept constant because at these pH values, the Ag-*g*-C_3N_4 and ACT have the same charge, and the repulsion force was dominant. Sun *et al.* [46] applied pH from 3.5 to 9 on N/S codoped/PMS system. The results showed that when the pH increased, the degradation was improving because the high concentration of OH^- caused the decomposition of PMS to produce $SO_4^{\cdot-}$. Ikhlaq *et al.* [50] studied the oxidation of ACT by using a zeolite/O_3 system at pH 3, 7, and 10. In this study, the optimum pH for zeolite/O_3 was 7.12 because, at this pH value, the ACT and hydroxyl groups on the zeolite surface were protonated. However, at pH 3 and 10, the oxidation of ACT decreased because ACT and zeolite at this pH have the same charge. Zhang *et al.* [52] studied the pH in the iron–copper bimetallic system activated by PS to remove ACT. The best pH values were between 5 and 7. The strong acid and alkaline conditions were not favorable for this system. Moreover, the effect of pH in Fe_3O_4 magnetic nanoparticles investigated by Tan *et al.* [53]. They reported that there were two effects of pH on the experiment: (1) Different PMS fractions would be affected by pH. In acidic conditions, HSO_5– predominated, while SO_4– predominated in alkaline conditions. (2) The electrostatic point of Fe_3O_4 had a pH effect on the catalyst surface charge of 7.3. At acidic pH, less PMS could catalyze on the catalyst surface because of the inhabitation effect of pH the H-bond formation between H^+ and O–O group of HSO_5 and positively charged catalyst surface. Kurniawan *et al.* [55] examined a wide range of pH values from 3 to 11 for ACT degradation using $BaTiO_3/TiO_2$/UVA. From pH 3 to 7, the degradation enhanced from 7 to 95%, and the optimum value for ACT oxidation was 7; meanwhile, in alkaline conditions, the degradation decreased from 95 to 54% because both the catalyst and the ACT molecules had negative charges in alkaline conditions. As a result, the catalyst's surface was repelled to the negatively charged ACT molecules, leading to a low ACT removal. Yaghmaeian *et al.* [56] investigated the influence of different pH to oxidize

ACT by using modified MgO nanoparticles catalyzed by ozone. They observed that the consumption of ozone was related to the increasing of pH: when the pH increased from 2 to 8, the consumption of ozone increased from 17 to 41.5%, and from 75 to 90% when the pH increased from 9 to 10. Also, more O_3 consumption means more OH production. $OH^{\cdot}$, has a high oxidation potential, which is more than O_3. The best pH value in this system was the natural pH solution close to 5.4; at this pH, the ACT molecule was mostly in its molecular form and could better interact with OH. In acidic conditions, there was no O_3 converted to $OH^{\cdot}$ enough. In the alkaline conditions, the isoelectric point of modified MgO and ACT were 10.4 and 9.4, respectively, which means the catalyst *m*-MgO significantly promoted the decomposition of O_3. In addition, Fan *et al.* [57] mentioned the influence of pH on the Ag/AgCl@ZIF8 system for oxidation of ACT. In this system, the optimum pH value was 5. The pH values between 7 and 9.4 were not desired because of weaker electrostatic integration between ACT and Ag/AgCl@ZIF8. For pH, more than 9.4 any pH values less than 7 were favorable for degradation ACT in this system. However, they noted that Ag/AgCl@ZIF8 dissolved in strong acid, which decreased the efficiency of this system for ACT removal. The influence of pH for decomposition of ACT in TiO_2@rGO nanoparticle system was studied by Cheshme Khavar *et al.* [59]. They revealed that when the pH increased from 4 to 9, the degradation of ACT promoted from 68 to 93%, respectively. Thus, it can be explained that at the natural pH solution, the surface catalyst has a negative charge, the anion species could not adsorb at the catalyst surface, allowing higher functional group interaction of OH^-, which resulted in a high amount of OH^- converting to $OH^{\cdot}$ and finally enhanced the degradation of ACT. Zhang *et al.* [63] observed that when the pH increased from pH 3 to 6.5, the degradation efficiency increased from 80 to 91%, respectively. In the acidic atmosphere, the oxidation of Fe^{2+} to Fe^{3+} was slower, according to the increasing of H^+, which inhabited the catalyst, resulting in a decrease in the degradation of ACT. When the initial pH value was 11, it has been observed that the pH decreased to be 3. They explained that because PS produced a large amount of H^+, the pH was drastically reduced. At pH 11, the OH^- molecules combined with Fe^{2+} caused a rapid reduction of Fe^{2+}, resulting in an insufficient coupling effect of Fe^{2+} and CuO, thus limiting the oxidation of ACT. Peng *et al.* [64] carried out different pH conditions. They revealed that pyrite/PDS could apply for a wide pH range, whereas pyrite/H_2O_2 in a narrow range. When pH 6 was implemented, the degradation of ACT in the pyrite/PDS system was 50%, whereas 0% when pyrite/H_2O_2 system was applied. Also, at pH 8, the results were 10 and 0%, respectively. It is believed that pH playing a central role in the determination of radical species of PDS, from pH 2 to 7 $SO_4^{\cdot-}$, from 8 to 10 $OH^{\cdot}/SO_4^{\cdot-}$, and from 10 to 12 $OH^{\cdot}$ was dominant. Also, Dong *et al.* [65] applied pH 3, 9, and 12. The results were 98.5, 79.5, and 13.5%, respectively. They observed, when the initial pH was 12, the pH value was decreasing to 3. This, because $SO_4^{\cdot-}$ would react with OH^- and H_2O resulting in the removal of H^+ and consumption of OH^-. In the base conditions, OH^- combined with Fe^{2+} to form oxyhydroxides and leads to precipitation. The absence of OH^- leading to insufficient activation of PS, which was due to a decrease in the degradation of ACT. Zhang *et al.* [66] also mentioned the influence of pH by using a S-doped graphene/Pt/TiO_2 system. When pH value increased from 4, 8, and 10, the removal was 99.9, 95.3, and 95.1%, respectively. In acidic conditions, hydroxyl radical behaved like a weak acid and reacted with hydroxyl ions under neutral and alkaline conditions, which was due to decreasing degradation reaction. The effect of pH on green rust coupled with Cu(II) has been reported by Zhao *et al.* [67]. They investigated three systems GR_{SO4}/Cu(II), GR_{CO3}/Cu(II), and GR_{Cl}/Cu(II), and it was observed that when pH 6 was applied on GR_{SO4}/Cu(II), and GR_{Cl}/Cu(II), the pH declined to 4, and 5.4, respectively. However, when pH 6 was applied to GR_{CO3}/Cu(II), the pH increased to 6.4 and then decreased to 4.2. This pattern may be due to the buffering effect of CO_3 in this H^+ system. Hydrolysis due to the rise in the pH, but as more accumulated, the buffering ability was exceeded, and then the pH decreased. When the pH decreased in the efficiency of GR_{SO4}/Cu(II) and GR_{CO3}/Cu(II) decreased from 100 to 82% and 84 to 28%, respectively.

4.4 The influence of scavengers

There are two mechanisms for the AOP: heterogeneous and homogeneous. In the mineral-based catalyst systems, oxidation mainly occurs on the catalyst surface; therefore, the heterogeneous reaction pathway is dominant. The mechanism of AOP is complex because some radical species are generating in parallel or series. To identify the radicals that are responsible for the degradation of ACT, the researchers added some substance called scavengers or quenching agents acting to trap the activated radicals: after adding these scavengers, the oxidation significantly declines, which means the radical trapped is responsible for the oxidation process. Table 4 represents the radicals generated in the AOP-synthesized particle-based system for degradation of ACT. Many scavengers such as isopropanol (IPA), *tert* butyl alcohol (TBA), methanol, salicylic acid, benzoquinone (BQ), KI (potassium iodide), triethanolamine (TEOA), ammonium oxalate, ethylenediaminetetracetic acid disodium (EDTA-2Na), ethanol (EtOH), sodium oxalate, N_2,

Table 4: Main superoxide species that generated during the degradation of ACT

Systems	Scavenger	Main radical	pH	Remarks	Ref.
C-modified TiO_2/ visible light	0.06 M IPA for $OH^{\cdot}$ 0.06 M BQ for $O_2^{\cdot-}$ KI for hole-capturer	$OH^{\cdot}$ and $O_2^{\cdot-}$	Neutral pH	When IPA and BQ were added, the degradation for ACT significantly decreased, which means that $OH^{\cdot}$ and $O_2^{\cdot-}$ were responsible of ACT degradation. Meanwhile, there was no effect for KI	[2]
Ag/ZnO@$NiFe_2O_4$/ PMS/UVA	Oxalate for h^+ TBA for $OH^{\cdot}$ EtOH for $OH^{\cdot}$ and $SO_4^{\cdot-}$ BQ for $O_2^{\cdot-}$	$O_2^{\cdot-}$, $SO_4^{\cdot-}OH^{\cdot}$, and h^+	7	All of the scavengers that were added to this system was significantly decreased the degradation of ACT	[38]
$CoFe_2O_4$/mpg-C_3N_4/PMS	TBA for $OH^{\cdot}$ EtOH for $OH^{\cdot}$ and $SO_4^{\cdot-}$	$SO_4^{\cdot-}$	7	There was a lower impact in the presence of TBA on the degradation of ACT	[39]
Solar light/Ag-*g*-C_3N_4/O_3	5 mM/L TBA for $OH^{\cdot}$ 5 mM/L TEOA for holes	Both of them were responsible for ACT degradation	7–9	When TBA and TEOH were added to the reaction, the oxidation decreased from 98 to 54.8 and 43.7%, respectively	[41]
N/S codoped ordered mesoporous carbon/PMS	EtOH for $SO_4^{\cdot-}$ *p*-BQ for $OH^{\cdot}$ L-His for $^1O_2$	Singlet oxygen and catalyst surface-bound reactive PMS complexes	3.5–9	The effect of EtOH and *p*-BQ on the degradation of ACT were neglected while L-His significantly inhibited the reaction	[46]
BiOCl/UVA	TBA for $OH^{\cdot}$ BQ for $O_2^{\cdot-}$ KI for $OH^{\cdot}$	$OH^{\cdot}$ and $O_2^{\cdot-}$	5.4	The obvious inhabitation in N_2 purging conditions verifies that $HO_2^{\cdot}/O_2^{\cdot-}$ originated from the reaction between DO and electron	[47]
OVPTCN/visible light	EDTA-2Na for holes *Tert*-butanol for $OH^{\cdot}$ *p*-BQ for $O_2^{\cdot-}$	$OH^{\cdot}$ was the main active radical, then holes	*	EDTA-2Na and *tert*-butanol were significantly affected on the ACT degradation, while *p*-BQ was a negligible effect	[49]
Iron–copper/PS	100 mM TBA for $OH^{\cdot}$ and $SO_4^{\cdot-}$ 100 mM methanol for $SO_4^{\cdot-}$	$SO_4^{\cdot-}$ and $OH^{\cdot}$	6.5	$SO_4^{\cdot-}$ was the main radical responsible for ACT oxidation, while $OH^{\cdot}$ just 20% from the total oxidation	[52]
Fe_3O_4 magnetic nanoparticles/PMS	EtOH TBA *Tert*-butanol Salicylic acid	Both of $SO_4^{\cdot-}$ and $OH^{\cdot}$	7	In the initial phase, only $OH^{\cdot}$ were generated, and then after 5 min or later, $SO_4^{\cdot-}$ started to generate	[53]
Ag/AGCl@ZIF8/visible light	1 mM AO for h^+ 1 mM IPA for $OH^{\cdot}$ 1 mM BQ for $O_2^{\cdot-}$	$O_2^{\cdot-}$	7	BQ inhabited the reaction significantly, which means $O_2^{\cdot-}$ was the main active substance responsible for the degradation of ACT	[57]
TiO_2@rGO/UV-LED	Methanol	$OH^{\cdot}$	5.4	The oxidation percentage declined from 81 to 34, 26, and 2% after the addition of methanol, *tert*-butanol, and salicylic acid, respectively	[59]

(*Continued*)

Table 4: *Continued*

Systems	Scavenger	Main radical	pH	Remarks	Ref.
Fe^{2+}/CuO/PS	TBA for $OH^{\cdot}$ Methanol for $SO_4^{\cdot-}$	$SO_4^{\cdot-}$ and $OH^{\cdot}$	6.5	After adding TBA and methanol, the removal declined to 79 and 89%, respectively	[63]
Pyrite/PDS and pyrite/H_2O_2	TBA for $OH^{\cdot}$ Ethanol for $SO_4^{\cdot-}$	$OH^{\cdot}$ was the dominant in pyrite/H_2O_2 and $SO_4^{\cdot-}$ was in pyrite/PDS system	4	H_2O_2 could not be generated at high pH, whereas PDS could be applied in wide pH ranges	[64]
CS-Fe/PS	Methanol $OH^{\cdot}$ and $SO_4^{\cdot-}$ TBA for $OH^{\cdot}$ Nitrobenzene for $SO_4^{\cdot-}$	$OH^{\cdot}$ and $SO_4^{\cdot-}$	7	TBA and NB exhibited slight inhabitation on ACT removal	[65]
Ferrous ion/copper oxide/O_2	BQ	$OH^{\cdot}$	3	After BQ was added, the degradation of ACT and the generation of H_2O_2 were completely suppressed	[71]
Fe/N-CNT/PS	MeOH and TBA	Nonradical pathway *via* electron transfer	5.5	*	[74]
ZnO/PSW/US/UV	tert-butanol	$OH^{\cdot}$	Natural pH	*	[73]
CNT10	IPA, BQ, and EDTA-2Na	h^+, $O_2^{\cdot-}$, and $OH^{\cdot}$	7	Oxidation of ACT by holes was the main oxidation mechanism, then $O_2^{\cdot-}$ and $OH^{\cdot}$ radicals	[75]
TiO_2 crystalline/UV	IPA	$OH^{\cdot}$	*	When IPA was added, the degradation of ACT completely suppressed	[76]
PAA/UVC-LED/Fe(II)	TBA, BQ, and MeOH	$OH^{\cdot}$	5	*	[82]
MNPs@C/UV/PMS	MeOH and TBA	$OH^{\cdot}$ and $SO_4^{\cdot-}$	6	The oxidation performance was decreased from 97.4 to 58 and 71.5% after addition of MeOH and TBA, respectively	[85]
B-Bi_2O_3/visible light	IPA for $OH^{\cdot}$ Sodium oxalate for h^+ TEMPOL for $O_2^{\cdot-}$ N_2 for DO	h^+ and $O_2^{\cdot-}$	*	When IPA was added, there was no change, whereas when sodium oxalate was added the degradation was affected significantly. Also, the degradation was a decline after TEMPOL and N_2 were added	[93]
Visible light/novel siligraphene/*g*-C_3N_4 composites	IPA, AO, and BQ	$OH^{\cdot}$, $O_2^{\cdot-}$, and h^+	Less than 6	The removal decreased to 44, 52, and 67% in the presence of IPA, BQ, and AO as $OH^{\cdot}$, $O_2^{\cdot-}$, and h^+ scavenger, respectively	[95]
Photo Fenton-like oxidation process	*p*-benzoquinone (*p*-BQ), 2-propanol, $AgNO_3$ and triethylamine	$O_2^{\cdot-}$	*	*	[96]
US/Fenton/TiO_2 NT process	*t*-BuOH	$OH^{\cdot}$	3	*	[99]
Bicarbonate-activated PS	Methanol, SOD, and FFA	Singlet oxygen ($^1O_2$)	8.3	The scavenger tests that none of the following radicals ($SO_4^{\cdot-}$ and $OH^{\cdot}$ nor superoxide $O_2^{\cdot-}$) was responsible for ACT degradation	[102]

(*Continued*)

Table 4: *Continued*

Systems	Scavenger	Main radical	pH	Remarks	Ref.
GAC/PS	MeOH and TBA	$SO_4^{\cdot-}$ $OH^{\cdot}$	3–7	Free radicals were not generated in the aqueous phase, whereas they were produced on the surface catalyst	[106]
CNT/PS		Electron transfer process		Scavengers were not affected on the ACT degradation	
Co-FeOCl/H_2O_2	TBA	Mainly $OH^{\cdot}$ and $O_2^{\cdot-}$ was detected	7	Methanol acting to trap superoxide radicals $O_2^{\cdot-}$	[107]
0.5-MnCN/PMS	EtOH, TBA, *p*-BQ, and FFA	$O_2^{\cdot-}$	6.5	The addition of TBA and EtOH, which were 1,000 times of the concentration of ACT, had negligible effects on ACT removal, whereas FFA and *p*-BQ were significantly inhibited the removal of ACT	[111]
CoAl-LDH/PMS	Electron paramagnetic resonance	$^1O_2$	6	*	[114]
SnO_2/O_3	*Tert*-butanol Salicylic acid Carbonate Chloride Sulfate Phosphate	$OH^{\cdot}$	7	*	[115]

*Means data not available.

4-hydroxy-2,2,6,6 tertamethylpiperidinyloxy (TEMPOL), and L-histidine (L-his) have been applied.

4.5 The influence of doping ratio

The impact of the doping ratio in the synthesized particles, such as TiO_2@rGO, Ag-*g*-C_3N_4, ZSM-5/TiO_2, $BaTiO_3$/TiO_2, La-doped ZnO, TiO_2/Fe_2O_3, Fe_3O_4@SiO_2, Mg/SiO_2, and iron-copper bimetallic doped with silica (Cu/Fe_3O_4@SiO_2), for the ACT removal has been investigated. Most of these studies agreed that when the doping ratio increases, the degradation of ACT increases. But if the doping ratio increased above the threshold, it might negatively impact the degradation performance. For example, Ling *et al.* [41] applied the Ag-*g*-C_3N_4 system to degrade ACT. The excessive amount of Ag might be accumulated on the *g*-C_3N_4 nanoparticle surface and cover the active sites, which increase the recombination of photogenerated charges. Lin and Yang [48] examined Cu-doped TiO_2 to eliminate ACT, many doping ratios were applied, 0.1, 1, and 10 wt%. The best result was 100% of ACT degradation within 3 h by using 0.1% of Cu. They revealed that when the Cu ratio increased, it may generate isolated CuO aggregates expelled from the Cu–TiO_2 framework to the pore channels, which may act as a center of charge recombination and decline the mass transport between the pore channels. Also, Kurniawan *et al.* [55] prepared $BaTiO_3$/TiO_2 composites catalyzed by solar irradiation. Three different ratios of $BaTiO_3$/TiO_2 were applied, composite-A (1:3), composite-B (1:1), and composite-C (3:1). After 4 h of reaction, the results were 76, 39, and 26%, respectively. Cheshme Khavar *et al.* [59] applied TiO_2@rGO nanocomposites catalyzed by UVA to oxidize ACT. Different doping ratios starting from 0, 1, 3, 5, 7.5, and 10 wt% of rGO were applied, and the degradation of ACT was 53, 83, 100, 87, 76, and 70%, respectively. These clearly showed that 3 wt% was the best doping ratio in the TiO_2@rGO system. If the doping ratio exceeds 3 wt%, the degradation efficiencies begin to decrease because a large amount of ACT adsorbs on the catalyst surfaces, which due to some occupied active sites of TiO_2 resulted in decreasing the UV light that reaches to TiO_2 surface and reduces the photocatalytic activity. In addition, when the UV transmission decreased by TiO_2, it might increase the recombination rate. Thi and Lee [68] observed that the presence of La doped on ZnO nanoparticles enhanced the photocatalytic activity and reduced the bandgap energy when applied 0.5 and 1.0 wt% La-doped ZnO. Meanwhile, too much adding like 1.5 wt% of La may adversely affect the system performance and increase the bandgap energy because, in each semiconductor, there is an energy level named Fermi, which is the highest energy level occupied by electrons in a particular site. In ZnO, the Fermi level is between the conduction band and valance band. When more than 1.0 wt% of La doped onto ZnO, the bandgap was increased because Burstein–Moss effect. These states could push the Fermi level to a higher energy position, and then the Fermi level would lie in the conduction band the process depicted in Figure 4.

Aziz *et al.* [69] studied TiO_2 doped onto fibrous silica ZSM-5 system catalyzed by solar light to oxidize ACT. Different doping ratios starting from 1, 3, and 5 wt%, of TiO_2 were carried out, and the results were 65, 90, and 71%, respectively. The results indicated that 3 wt% was the best doping ratio in the ZSM-5/TiO_2 system. They explained that TiO_2 might agglomerate on the surface of fibrous silica and cover the active sites, which caused low penetration of the visible irradiation. This effect was detected when electron carrier concentration exceeded

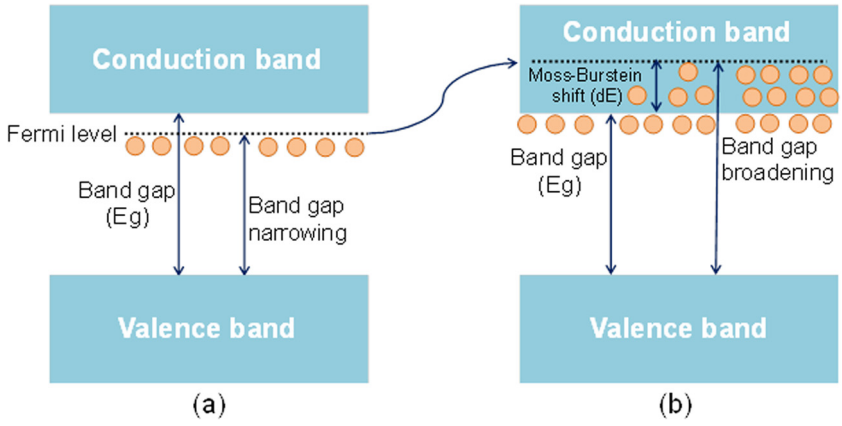

Figure 4: (a) Band gap narrowing of 0.5–1.0 wt% La-doped ZnO, and (b) band gap broadening for 1.5 wt% of La-doped ZnO.

the conduction band edge density of the state. However, some studies did not observe any decreases with an increase in the doping ratio. For example, Da Silva *et al.* [40] applied Mg/SiO_2/UV system. Many Mg concentrations experimented with to oxidize ACT, 1, 2, 10, and 25 wt%. The best result was 60% of ACT was removed within 60 min obtained when 25 wt% Mg concentration was applied. Moreover, Abdel-Wahab *et al.* [60] applied TiO_2/Fe_2O_3 with different TiO_2 ratios, 15, 33, and 50 wt%. They observed that when the concentration of TiO_2 increased from 15 to 50%, the degradation increased from 52.5 to 98%, respectively. The improvement of ACT degradation could be correlated to the effective separation of photogenerated electron–hole pairs accomplished by a combination of narrow bandgap Fe_2O_3 with wide bandgap TiO_2. In addition, the oxidation rate of ACT was accelerated proportionally when increasing copper concentration from 0 to 1% in Cu/Fe_3O_4@SiO_2 system, and the degradation increases from 59.2 to 100%, respectively. That was because ACT could quickly and efficiently adsorb on the catalyst and thus increase the catalyst activity. Do *et al.* [51] observed that when the molar ratio of Cu increased from 2.1 to 2.94, the reaction rate begins to slow down because of the dispersion morphology of Cu nanocomposites of the surface of iron doped with silica (Fe_3O_4@SiO_2).

4.6 The influence of oxidants dosage

The influence of addition and the concentrations of PMS, PS, oxygen (O_2), ozone (O_3), and hydrogen peroxide (H_2O_2) have been widely investigated. All the studies agreed that the addition of oxidants enhances the degradation and the reaction rates of ACT. However, when an excessive amount of oxidant is added, it may impact adversely on the degradation performance. This attributed to many reasons: (1) the excessive amount of oxidants generate more radicals, these radicals may consume each other as shown in the Eqs. (46–50):

$$OH^{\cdot} + OH^{\cdot} \rightarrow H_2O \quad (46)$$

$$SO_4^{\cdot -} + SO_4^{\cdot -} \rightarrow S_2O_8^{2-} \quad (47)$$

$$SO_4^{\cdot -} + OH^{\cdot} \rightarrow HSO_4^{-} + \frac{1}{2}O_2 \quad (48)$$

$$HSO_5^{-} + OH^{\cdot} \rightarrow SO_5^{\cdot -} + H_2O \quad (49)$$

$$HSO_5^{-} + SO_4^{\cdot -} \rightarrow SO_4^{\cdot -} + SO_4^{2-} + H^{+} \quad (50)$$

(2) The limitation of active sites on the catalyst surface according to the presence of a high concentration of oxidant, and (3) if the excessive concentration of H_2O_2 was added, the generated hydroxyl radicals may react with H_2O_2 to produce $HO_2^{\cdot}HO_2^{\cdot}$, which contributed less oxidation potential than $OH^{\cdot}$. Several studies investigated the addition of oxidant in AOP based on composites systems. Ziylan-Yavaş and Ince [17] observed that when the ozone flow increased from 3, 6, and 9 mg/min on Pt/Al_2O_3/O_3 system, the oxidation was enhanced, and 9 mg/min contributed the best ozone flow in this system. That may refer to the excessive amount of H_2O_2 produced from the oxidation of ozone, which in turn increases the $OH^{\cdot}$ that attacks ACT resulting in an increased ACT degradation. Hassani *et al.* [39] also examined different PMS dosages in $CoFe_2O_4$/mpg-C_3N_4 catalyzed by PMS to degrade ACT. At 0.5 mM of PMS, the degradation efficiency was 60.9% after 25 min reaction. At 1.5 mM of PMS, the efficiency increased to 92%. They mentioned that higher PMS concentration was not favorable in this system because of the reasons mentioned above. Moreover, Sun *et al.* [46] examined many concentrations of PMS on N/S codoped ordered mesoporous carbon system. When 0.25, 0.5, and 1.0 mM of PMS were applied, the k values increased from $2.0 \pm 0.04 \times 10^{-2}$ to $2.4 \pm 0.06 \times 10^{-1}$ and $3.7 \pm 0.2 \times 10^{-1}$, respectively. Also, Wang *et al.* [47] pointed out the addition of $Na_2S_2O_8$ and H_2O_2 on the BiOCl/UVA system. When $Na_2S_2O_8$ was added, the degradation rate and the mineralization were accelerated and enhanced. They attributed the improvement to three reasons: (1) the direct reaction between the photon and PS molecules, which results in generating sulfate radicals, (2) also, PS may react with conduction band electrons yielding the formation of sulfate radicals, and (3) sulfate radicals may generate from the reaction of $O_2^{\cdot -}$ with PS. However, when H_2O_2 was added, the total organic carbon (TOC) removal was slowed down because the higher O–O the bond energy of H_2O_2 compared with the band in the free PS ions under the natural pH might interpret why PS was easier to activate than H_2O_2. Zhang *et al.* [52] studied the effect of different PS dosages, from 0.2 to 0.6 g/L, on the Fe_2O_3@Cu_2O system to degrade ACT. They noted that a further increase in PS concentration might be less effective because sulfate radicals consumed each other. Tan *et al.* [53] studied the influence of adding different PMS concentrations on the degradation rate in Fe_3O_4 magnetic nanoparticles/PMS system. They observed that when the initial concentration of PMS increased from 0.0 to 0.2 mM, the reaction rate was promoted from 0.23×10^{-2} to 1.22×10^{-2}/min. However, when the initial concentration of PMS increased from 0.2 to 0.5 mM, the reaction rate slightly decreased from 1.45×10^{-2} to be 1.13×10^{-2}/min. The increase of degradation rate in the initial concentration 0.2 mM was attributed to the availability of PMS. At this concentration,

PMS acting as a limiting factor controlling the yield of radicals. Furthermore, Tan *et al.* [58] applied different PMS dosages on $MnFe_2O_4$ and $CoFe_2O_4$ to eliminate ACT. The dosages were 0.05, 0.1, 0.15, and 0.2 g/L, and the removal of ACT when $MnFe_2O_4$ and $CoFe_2O_4$ were used were 89, 100, 100, 100% and 55.6, 85.7, 94, 100%, respectively. They noted that when the initial concentration of PMS increased to 0.4 mM, the degradation rate started to decline. In this study, there was no adverse effect observed because the initial concentration of PMS did not reach the threshold level. Dong *et al.* [65] mentioned that when higher PS concentration applied, PS got in the micropores in the catalyst and would react with $SO_4^{\cdot -}$ and led to PS consumption, thereby causing the undesired inhibiting effect. In addition, Velichkova *et al.* [70] demonstrated that at 153 mM of H_2O_2 in MGN1, MGN2, and MGM systems, the reaction efficiency started to decrease, according to the reaction of $OH^{\cdot}$ with H_2O_2 as shown in equation (51):

$$OH^{\cdot} + H_2O_2 \rightarrow H_2\,O + HO_2^{\cdot} \quad (51)$$

As mentioned above, $HO_2^{\cdot}$ contributed less oxidation potential than $OH^{\cdot}$, which adversely affect the degradation performance.

4.7 The influence of oxygen

The impact of the oxygen for ACT degradation by using AOP based on composites has been investigated. Moctezuma *et al.* [8] revealed that oxygen has a strong effect on photocatalytic degradation. Bubbling O_2 acted to trap the free electrons to inhabit the recombination of (e^-/h^+), which affect positively on the degradation performance. Also, Yang *et al.* [44] reported that O_2 increased the degradation of ACT more than six times. O_2 could inhabit electron–hole recombination as O_2 consumes conduction band electrons allowing valance band holes too, directly and indirectly as shown in Eqs. (52)–(55).

$$O_2^{\cdot -} + H^+ \rightarrow HO_2^{\cdot} \quad (52)$$

$$HO_2^{\cdot} + H^+ + e_{cb}^- \rightarrow H_2O_2 \quad (53)$$

$$H_2O_2 + e_{cb}^- \rightarrow OH^{\cdot} + OH^- \quad (54)$$

$$H_2O_2 + hv \rightarrow O_2^{\cdot -} \quad (55)$$

Zhang *et al.* [52] demonstrated that low O_2 concentration resulted in a lower ACT oxidation rate in the iron–copper/PS system. Also, the dissolved oxygen (DO) in the solution related adversely with N_2 purging, which decreased $SO_4^{\cdot -}$ resulted in the decrease of ACT oxidation. It should be noted that the formation of $O_2^{\cdot -}$ through the reduction of O_2 by photoinduced electrons in the conduction band and subsequent inhabitation of (e^-/h^+) recombination. Furthermore, $O_2^{\cdot -}$ may react and generate more oxidizing species such as $OH^{\cdot}$, H_2O_2, and $HO_2^{\cdot}$. Moreover, a high concentration of oxygen and a small amount of UV 185 nm induce the formation of O_3 followed by the generation of H_2O_2 to produce more $OH^{\cdot}$. Abdel-Wahab *et al.* [60] examined two oxygenating systems: (1) static O_2 atmosphere and (2) purging 100 mL/min of O_2. The results showed that after 90 min of reaction, the removal of ACT was 75 and 99%, respectively. The enhancement in the degradation performance may be attributed to the formation of $O_2^{\cdot -}$ by photoinduced electrons in the conduction band and subsequent inhabitation of (e^-/h^+) recombination. Furthermore, $O_2^{\cdot -}$ may react and generate more oxidizing species such as $OH^{\cdot}$, H_2O_2, and $HO_2^{\cdot}$. Zhang *et al.* [63] investigated the effect of DO in the degradation of ACT by using Fe^{2+}/CuO/PS system. The result showed that the degradation decreased from 92 to 70% when the system purged with N_2, which means that oxygen played a major role in this system. As DO decreased, $O_2^{\cdot -}$, which functioned between and Cu^{2+} and Cu^+, decreased according to Eqs. (56)–(59). Thus, resulting in a decrease in $OH^{\cdot}$, which was due to a decline in the degradation of ACT.

$$Cu^+ + O_2 \rightarrow Cu^{2+} + O_2^{\cdot -} \quad (56)$$

$$Cu^+ + 2H^+ + O_2^{\cdot -} \rightarrow Cu^{2+} + H_2O_2 \quad (57)$$

$$Cu^+ + H_2O_2 \rightarrow Cu^{2+} + OH^{\cdot} + OH^- \quad (58)$$

$$Cu^{2+} + O_2^{\cdot -} \rightarrow Cu^{2+} + O_2 \quad (59)$$

Zhang *et al.* [71] pointed out, that DO plays an important role in the oxidation of ACT and for radical's generation when Fe^{2+}/CuO was applied. When Fe^{2+}/CuO was added, the concentration of DO decreased from 9.48 to 4.85 mg/L in the first 10 min of reaction and then increased to 7.64 mg/L after 6 h reaction. In addition, they observed that the removal of DO completely inhibits the degradation of ACT.

4.8 The influence of temperature

According to the literature, the temperature is directly proportional to the removal of pollutant because the pollutant migrates from the bulk solution to the gas–liquid interface region where temperature and $OH^{\cdot}$ are high. Moreover, it has been proposed that the optimum temperature was based on the characteristic of organic matter and the kinetics of the reaction between $OH^{\cdot}$ and pollutant. Velichkova *et al.* [70] studied the effect of temperature

Table 5: Summary of the studies that applied degradation cycles to examine the durability of the catalysts

Catalysts	Running times	Remarks	Ref.
Carbon-doped Ti calcinated at 500°C air	4	No considerable loss of activity after four cycles	[2]
MgO	4	The efficiency dropped from 99.3 to 90%	[3]
1.0% w/w Ag/ZnO 0.04@$NiFe_2O_4$	4	The degradation was 100, 100, 100, and 95%, respectively. Also, there was a small amount of leaching in Ag, Fe, Ni, and Zn	[38]
$CoFe_2O_4$ mpg-C_3N_4 nanocomposite	3	During the three degradation cycles, the degradation performance was constant, but in the fourth cycle, the performance dropped according to the leaching of iron and cobalt	[39]
4% Ag-*g*-C_3N_4/O_3	4	The mineralization efficiency slightly dropped from 83.1 to 79.9%	[41]
0.2-TFSZ	5	After the fifth cycle, the removal declined from 96 to 84%. The decline may attribute to the loss of catalyst mass during the recycling	[43]
NS-CMK-3	5	This catalyst showed superior stability and the degradation percentage was kept constant at 98%	[46]
0.1 wt% Cu-doped TiO_2	10	The efficiency was still constant even after ten times of repetitions	[48]
OVPTCN	4	There was a negligible decrease in ACT removal after four running times. Also, a trace amount of was TiO_2 leached	[49]
Fe_3O_2@SiO_2-Cu 1.04	6	This catalyst showed superior stability and the degradation percentage was kept constant at 100% within 60 min after six degradation cycles	[51]
Fe_2O_4 magnetic nanoparticles	4	The reaction rates decreased after each recycles. The degradation was 74.7, 51.9, 39.7, and 29.5%, respectively	[53]
Ag/AgCl at ZIF-8	3	After three times of reaction, the degradation rate decreases just 5% without any change in the catalyst morphology	[57]
$MnFe_2O_4$ And $CoFe_2O_4$	3	After 60 minutes, the degradation of $MnFe_2O_4$ Composites was 100% for all cycles. $CoFe_2O_4$ removal rates were 100, 85.4, and 67.1%, respectively.	[58]
TiO_2@rGO	5	Five successive recycles with little decrease in degradation. The degradation after fifth recycle was 88%	[59]
33% TiO_2/Fe_2O_3	5	After the fourth cycle, there was no change in the catalyst performance. But in the fifth cycle, the degradation declined to 57.5%	[60]
Hollow mesoporous TiO_2	10	After ten times, there was no significant deactivation	[61]
Pyrite	4	In both systems, after each run, the catalyst lost around 5% of its weight. The removal efficiency after four cycles was 90%	[64]
CS-Fe	5	Still above 90% after the fifth cycle	[65]
MGN1, MGN2, and MGM	2	All catalyst demonstrated a good stability	[70]
Ferrous ion and copper oxide	3	After three times of recycles, the efficiency dropped according to the leaching of copper or/and accumulation of iron precipitates	[71]
ZnO/PSW	4	For the first three running times, the oxidation percentage just declined 10%, whereas at the end of the fourth cycle, the efficiency decreased 20%	[73]
Fe/N-CNT	10	ACT degradation percentage kept at 99.8% after the tenth cycle	[74]
TiO_2 thin films calcinated at 650°C	1	After 6 hrs of reaction, there was no significant change in ACT oxidation	[78]
Cu/Fe-PILC	2	Only 3% of losing in mineralization efficiency	[80]
MNPs@C	5	After five running times, the degradation decreased to 91%, which reflects good catalyst stability	[85]
ZnO-Z and TiO_2-Z	4	A slight decline in efficiency has been observed%	[87]
	4		[88]

(*Continued*)

Table 5: *Continued*

Catalysts	Running times	Remarks	Ref.
3% (w/w) of WO_3/TiO_2/SiO_2 composite		There was a slight change in the degradation performance after fourth running time	
Novel siligraphene/g-C_3N_4 composites	5	There was a slight decrease after five cycles which confirms the good durability of the catalyst composites	[95]
UiO-66-NH_2	30 h	After 30 h of reaction, the catalyst has shown good stability	[96]
GAC and CNT	5	The decomposition of ACT was more than 80% after the fifth cycle	[106]
Co-FeOCl	3	ACT oxidation performance significantly declined from the second run 87.5 to 41.3%, whereas there was no significant change after the third cycle	[107]
TCuO50-GO	3	After three running times, the degradation efficiency is still more than 95%	[108]
Fe-SBA-15(20)$FeCl_3$ and Fe-SBA-15(20)$Fe_2(SO_4)_3$ MNPs/β-CD/$KMnO_4$	3	After the third cycle the efficiency dropped from 87 to 80%	[109]
	5	After the fifth cycle, the degradation percentage slightly decreased from 94.6 to 84.4%	[110]
ZVC	6	After the sixth cycle, the degradation percentage decreased 23%	[112]
CoAl-LDH	4	Between the first and fourth cycles, the degradation efficiency just decreased less than 3%	[114]
SnO_2	4	After the fourth cycle, the ACT oxidation was not change significantly	[115]
Cr/MCM-41 and Fe/MCM-41	7 days	After the seventh day of reaction, the catalyst was capable to maintain a high degradation performance	[116]
Mn_2O_3	3	The degradation was 98, 81.5, and 76.2%. No observable change in the morphology	[117]
Fe_3O_4@SiO_2@Cu	6	There was no observable decline in the degradation efficiency after the sixth running time	[118]

on the degradation of ACT by three types of nanoparticles of iron oxide/H_2O_2 system. They revealed that the increase in the temperature from 30 to 60°C had a beneficial effect for all examined conditions. Also, a higher temperature increases the rate of $OH^{\cdot}$ formation. In contrast, high temperature increases the decomposition of H_2O_2 into O_2 and water, which reduces the removal efficiency of ACT. In addition, Im *et al.* [72] studied the effect of temperature on the removal of ACT by ultrasound. Two ultrasound waves were applied at 28 and 1,000 kHz, and the best temperature was 25 and 35°C, respectively. They mentioned that beyond the optimum temperature leads to an increase in bubble vapor and then bubble collapse due to the reaction of net energy and free radicles. Tan *et al.* [53] applied different temperatures from 30 to 70°C in Fe_3O_4 magnetic nanoparticles/H_2O_2 and PMS system. The results showed that temperature affects positively on the elimination of ACT and the kinetic increased from 1.5×10^{-2} to 10×10^{-2}/min, for 30 and 70°C, respectively. In addition, Sun *et al.* [46] reported that when N/S codoped ordered mesoporous carbon was applied for ACT degradation at 25°C, the removal was 100% after 30 min, whereas at 45°C, ACT was completely degraded after 20 min, and the kinetic at 25 and 45°C were 2.4×10^{-1} and 3.5×10^{-1}/min, respectively. The activation energy, E_a, of the oxidation system was calculated as 13.8 kJ/mol, which suggested the reaction temperature does not have a significant effect on the oxidation reaction.

5 Stability and reusability of the catalysts

One of the main advantages of synthesized particles, which use in AOP systems, is their durability and reusability without any considerable change in the degradation performance. According to the literature, the reduction in the degradation efficiency attributes to the following reasons: (1) metals such as Ag, Zn, Fe, Cu, and Ni could be

Table 6: Summary of the main byproducts that detected after ACT degradation

Systems	Byproducts	Ref.
Modified MgO nanoparticles catalyzed by O_3	Carboxylic acid derivatives were the main byproducts such as malonic acid, succinic acid, malic acid, formic acid, hydroxy-acetic acid, acetamide, and nitrite	[3]
UV-TiO_2	*p*-Aminophenol and *p*-nitrophenol	[8]
Ultrasound/Pt-supported nanocomposites of Al_2O_3	Small carboxylic compounds	[17]
1.0% w/w Ag/ZnO 0.04@$NiFe_2O_4$/PMS/UVA	Acetic acid, 1,2 dihydroxyldenzene, glycolic acid, *a*-hydrogen acid, 1,4-benzoquinone, and 3-hydroxypropanic acid	[38]
Solar/4% Ag-*g*-C_3N_4/O_3	1,4-Hydroquinone, dihydroxylated or trihydroxylated	[41]
UV-TiO_2	Formic acid, oxamic acid, acetamide, hydroxy-acetic acid, malonic acid, butenedioic acid, succinic acid, malic acid, hydroquinone, acetamide, *N*-(2,4-dihydroxyphenyl), acetamide, *N*-(3,4-dihydroxyphenyl)	[44]
TiO_2 nanotube/UV	Formic acid, oxamic acid, and oxalic acid	[45]
OVPTCN/visible light	Hydroquinone, 1,4-benzoquinone, 4-methoxyphenol, 2-hexenoic, and malic acid	[49]
Photocatalytic/$BaTiO_3/TiO_2$	Hydroquinone and 1,4-benzoquinone	[55]
Ag/AgCl at ZIF-8/visible light	Salicylaldehyde, acetamide and phenol, lactic acid, succinic acid, malic acid, and maleic acid	[57]
Photocatalytic/15% TiO_2/Fe_2O_3	4-Acetamidoresorcinol, 4-acetamidocatechol, 1,2,4-benzentriol, hydroquinone, acetamide, carboxylic acid derivatives have been observed like tartaric acid, malic acid, maleic acid, succinic acid, malonic acid, oxalic acid, and oxamic acid	[60]
Photocatalytic of hollow mesoporous TiO_2	Oxalic acid and oxamic acid	[61]
Fe_2O_3@Cu_2O/PS	*N*-(Aminocarbonyl)-acetamide, hydroquinone acetate, and 2-pentanol acetate	[63]
PDS/pyrite	Hydroquinone, acetamide, acetic acid, and nitric acid	[64]
H_2O_2/pyrite	Hydroquinone, acetamide, acetic acid, and nitrate	
CS-Fe/PS	1,4-Dihydroxyl benzene, *p*-BQ, and *p*-hydroxyphenol	[65]
Photocatalytic of 1% La-doped ZnO	Hydroquinone, oxamic acid, acetic acid, butyric acid, 2-amino-5-methyl benzoic acid, and benzoic acid	[68]
Ferrous ion and copper oxide	Hydroquinone, ammonium, carboxylic acid derivatives; oxalic acid, formic acid, and acetic acid	[71]
Fe/N-CNT/PS	Oxaloacetic acid and 4-nitrophenol	[74]
Solar photocatalytic of TiO_2	Acetic acid, oxalic acid, maleic acid, propionic acid, pyruvic acid, and formic acid	[77]
Photo Fenton process catalyzed by a Cu/Fe-PILC	1,2-Benzoquinone, 1,4-benzoquinone, oxamic acid, acetamide, and hydroquinone	[80]
PAA/UVC-LED/Fe(II)	4-Nitrophenol and hydroquinone	[82]
Photocatalyst/β-Bi_2O_3	Hydroquinone, formic acid, succinic acid, and hydroxy-acetic acid	[93]
Photo-Fenton	Acetate, oxalate, formate, and propionate	[92]
Photo-Fenton solar process/synthesized wastewater	Hydroquinone and monohydroxilated derivative	[94]
Solar light/Fe_2O_3–TiO_2 nanocomposites	Acetic acid, oxamic acid, oxalic acid, butyric acid, acetamide, and hydroquinone	[97]
Zero-valent aluminum under air-equilibrated acidic conditions	Hydroquinone and anion derivatives; nitrate, acetate	[101]
Fenton oxidation	Hydroquinone, benzaldehydes, benzoic acids, include alcohols, ketones, aldehydes, and carboxylic acids	[103]
Fenton process	*p*-BQ, hydroquinone (1,4-dihydroxybenzene), catechol (1,2-dihydroxybenzene), resorcinol (1,3-dihydroxybenzene), and 2,4-dinitrophenol	[104]
Aerated Fenton reactor	Oxalic acids	[105]
0.5-MnCN/PMS	Hydroquinone, acetyl, and aminophenol	[111]
TiO_2-rGO 5%/plasma	Hydroquinone, 4-methoxyphenol, malic acid, 4-heptanol, and 2-hexenoicacid	[112]
ZnO/PSW-contained sono-reactor was irradiated by UVC light	Hydroquinone, oxalic acid, formic acid, acetic acid, and ammonium	[113]
SnO_2/O_3	Carboxylic acids	[115]
Fe/MCM-41 and Cr/MCM-41/Catalytic wet peroxide oxidation	Oxalic acid, acetic acid, and formic acid	[116]
Direct electron transfer by reactive Mn_2O_3	Acetic acid and *a*-nitrosophenol	[117]

leaching during the reaction, or/and (2) loss of the catalyst weight during the regeneration, or/and (3) agglomeration during the reaction. Most applied experiments using the following procedure to recover the catalyst: washing the catalyst three times with deionized water and dry them at a temperature between 80 and 100°C for 24 h. Sun *et al.* [46] used NS-CMK-3 catalyst to remove ACT. After five times of running, the catalyst showed high durability to oxidize ACT from an aqueous medium. Soltani *et al.* [73] applied ZnO/PSW nanopowder for four times to remove ACT. The authors revealed the first three times of running, the catalyst showed good stability, whereas at the end of the fourth cycle, the efficiency decreased to 20%. Moreover, Pham *et al.* [74] examined the durability of Fe/N-CNT particles to degrade ACT. Palas recovered and reused the catalyst for ten times. The catalyst showed superior stability even after ten times of degradation cycle, the oxidation efficiency was kept as 99.8%. In the Table 5, some studies have examined the catalyst for many cycles to oxidize ACT.

6 Byproducts formation

As mentioned in the introduction, some ACT byproducts such as 1,4-benzoquinone and *N*-acetyl-*P*-benzoquinone have negative effects on human health. Most of the byproducts mainly consist of hydroquinone and carboxylic acid derivatives. Ling *et al.* [41] applied $Ag-G-C_3N_4/O_3$ catalyzed by Vis-UV light to oxidize ACT from a liquid medium. After the degradation process, the main byproducts were hydroquinone, di-hydroxyphenyl, and tri-hydroxyphenyl. Moreover, Montenegro-Ayo *et al.* [45] observed small byproducts such as formic acid, oxamic acid, and oxalic acid after ACT oxidation by using TiO_2/UV system. In addition, Zhang *et al.* [71] detected oxalic acid, hydroquinone, formic acid, acetic acid, and ammonium as byproducts after ACT degradation by using ferrous ion and copper oxide/O_2 system. Table 6 lists the studies, which monitored the byproducts of ACT after treatment processes.

7 Conclusions and future prospective

This review article has attempted to cover a wide range of state-of-the-art studies related to the oxidation of ACT by using semiconductor and metal catalysts. Hydroxyl radical was the most dominant superoxide responsible for ACT degradation because hydroxyl radical could be generating in all AOP systems, such as ultrasound systems, photocatalytic systems, and AOP-based oxidants systems, that were investigated for ACT degradation. Also, the stability and reusability of the catalysts have been studied. Most of the semiconductor catalysts have shown good stability, but Fe and N codoped carbon nanotube/PS system have shown superior stability, and the degradation efficiency is still 99.8% after the tenth cycle. pH has played a central role in ACT degradation by control of zero of point charge of the catalyst, pK_a of ACT, and the formation of radicals. In addition, the influence of catalyst, ACT, and oxidant concentrations has been reported. The increase of catalyst concentration was beneficial, but if the catalyst concentration exceeds the threshold point, it adversely impacted the degradation efficiency. Because of high catalyst concentrations, the agglomeration and the shielding effect of the suspended catalyst are due to increased turbidity and low light penetration, which reduces the accessible light to the catalyst surface resulting in decreased photocatalytic activity. High catalyst concentration leads to an increase in the number of activated radicals, which results in the self-consumption of generated radicals. If excessive amount of ACT was added that is due to, for systems based on oxidants such as hydrogen peroxide, PS, and PMS, high ACT concentrations may adsorb and cover a wide number of the active sites on the catalyst's surface consequently, suppresses the production of super oxidant radicals. Moreover, for the systems that depend on UV or visible lights as a catalyst, a high ACT concentration may accumulate on the catalyst surface and prevent the penetration of the irradiation, which may reduce the photocatalytic efficiency. For oxidants, the excessive amount of oxidants (1) generate more radicals, which may consume each other, (2) the limitation of active sites on the surface catalyst according to the presence of a high concentration of oxidant, and (3) if the excessive concentration of H_2O_2 was added, the generated hydroxyl radicals might react with H_2O_2 to produce $HO_2^{\cdot}$, which contributed less oxidation potential than $OH^{\cdot}$. It has been noted that the increase in doping ratio was not beneficial because the agglomerate on the surface covers the active sites, which caused low penetration of the irradiation. The studies agreed that DO improved ACT degradation, which attributed to the reaction between O_2 and generated radical yielding to the formation of superoxide radicals. A high degree of temperature was not good for ACT degradation because high temperature increases the decomposition of H_2O_2 into O_2 and water, which reduces

the removal efficiency of ACT. Finally, most of the byproducts mainly consist of hydroquinone and carboxylic acid derivatives. AOP systems based on micro and nanoparticles are considered a promising method for ACT degradation. There is a deficiency in the literature about the prediction of the oxidation mechanism of ACT in the presence of nanomaterials. This topic needs further investigation. In addition, the threshold of concentrations and the ratio of oxidants, pollutants, and catalysts need further investigation to expect the optimum ratio between them.

Funding information: The authors would like to express their appreciation to the Ministry of Higher Education Malaysia for the Fundamental Research Grant Scheme with Project Code: FRGS/1/2019/STG07/USM/02/12.

Author contributions: All authors have accepted responsibility for the entire content of this manuscript and approved its submission.

Conflict of interest: The authors state no conflict of interest.

References

[1] Thomaidi VS, Stasinakis AS, Borova VL, Thomaidis NS. Is there a risk for the aquatic environment due to the existence of emerging organic contaminants in treated domestic wastewater? Greece as a case-study. J Hazard Mater. 2015;283:740–7.

[2] Gómez-Avilés A, Peñas-Garzón M, Bedia J, Rodriguez JJ, Belver C. C-modified TiO_2 using lignin as carbon precursor for the solar photocatalytic degradation of acetaminophen. Chem Eng J. 2019;358:1574–82.

[3] Mashayekh-Salehi A, Moussavi G, Yaghmaeian K. Preparation, characterization and catalytic activity of a novel mesoporous nanocrystalline MgO nanoparticle for ozonation of acetaminophen as an emerging water contaminant. Chem Eng J. 2017;310:157–69.

[4] Dai G, Huang J, Chen W, Wang B, Yu G, Deng S. Major pharmaceuticals and personal care products (PPCPs) in wastewater treatment plant and receiving water in Beijing, China, and associated ecological risks. Bull Env Contam Toxicol. 2014;92(6):655–61.

[5] Wang S, Wu J, Lu X, Xu W, Gong Q, Ding J, et al. Removal of acetaminophen in the Fe^{2+}/persulfate system: kinetic model and degradation pathways. Chem Eng J. 2019;358(May 2018):1091–100.

[6] Bound JP, Voulvoulis N. Pharmaceuticals in the aquatic environment – A comparison of risk assessment strategies. Chemosphere. 2004;56(11):1143–55.

[7] Zwiener C, Frimmel FH. Oxidative treatment of pharmaceuticals in water. Water Res. 2000;34(6):1881–5.

[8] Moctezuma E, Leyva E, Aguilar CA, Luna RA, Montalvo C. Photocatalytic degradation of paracetamol: intermediates and total reaction mechanism. J Hazard Mater. 2012;243:130–8.

[9] Cabrera-Reina A, Miralles-Cuevas S, Oller I, Sánchez-Pérez JA, Malato S. Modeling persulfate activation by iron and heat for the removal of contaminants of emerging concern using carbamazepine as model pollutant. Chem Eng J. 2020;389:124445.

[10] Phillips PJ, Smith SG, Kolpin DW, Zaugg SD, Buxton HT, Furlong ET, et al. Pharmaceutical formulation facilities as sources of opioids and other pharmaceuticals to wastewater treatment plant effluents. Env Sci Technol. 2010;44(13):4910–6.

[11] Do QC, Kim DG, Ko SO. Controlled formation of magnetic yolk-shell structures with enhanced catalytic activity for removal of acetaminophen in a heterogeneous fenton-like system. Env Res. 2019;171:92–100.

[12] Ebele AJ, Abou-Elwafa Abdallah M, Harrad S. Pharmaceuticals and personal care products (PPCPs) in the freshwater aquatic environment. Emerg Contam. 2017;3(1):1–16.

[13] Amouzgar P, Chan ES, Salamatinia B. Effects of ultrasound on development of Cs/NAC nano composite beads through extrusion dripping for acetaminophen removal from aqueous solution. J Clean Prod. 2017;165:537–51.

[14] Nikolaou A, Meric S, Fatta D. Occurrence patterns of pharmaceuticals in water and wastewater environments. Anal Bioanal Chem. 2007;387(4):1225–34.

[15] Liu JL, Wong MH. Pharmaceuticals and personal care products (PPCPs): a review on environmental contamination in China. Env Int. 2013;59:208–24.

[16] Skoumal M, Cabot PL, Centellas F, Arias C, Rodríguez RM, Garrido JA, et al. Mineralization of paracetamol by ozonation catalyzed with Fe^{2+}, Cu^{2+} and UVA light. Appl Catal B Env. 2006;66(3–4):228–40.

[17] Ziylan-Yavaş A, Ince NH. Catalytic ozonation of paracetamol using commercial and Pt-supported nanocomposites of Al_2O_3: the impact of ultrasound. Ultrason Sonochem. 2018;40:175–82.

[18] Sim WJ, Lee JW, Oh JE. Occurrence and fate of pharmaceuticals in wastewater treatment plants and rivers in Korea. Env Pollut. 2010;158(5):1938–47.

[19] Roberts PH, Thomas KV. The occurrence of selected pharmaceuticals in wastewater effluent and surface waters of the lower Tyne catchment. Sci Total Env. 2006;356(1–3):143–53.

[20] Llamas-Dios MI, Vadillo I, Jiménez-Gavilán P, Candela L, Corada-Fernández C. Assessment of a wide array of contaminants of emerging concern in a Mediterranean water basin (Guadalhorce river, Spain): motivations for an improvement of water management and pollutants surveillance. Sci Total Env. 2021;788:147822.

[21] Moussavi G, Momeninejad H, Shekoohiyan S, Baratpour P. Oxidation of acetaminophen in the contaminated water using UVC/$S_2O_8^{2-}$ process in a cylindrical photoreactor: efficiency and kinetics of degradation and mineralization. Sep Purif Technol. 2017;181:132–8.

[22] Degefu DM, Weijun H, Zaiyi L, Liang Y, Zhengwei H, Min A. Mapping monthly water scarcity in global transboundary basins at country-basin mesh based spatial resolution. Sci Rep. 2018;8(1):1–10.
[23] Rathi BS, Kumar PS. Application of adsorption process for effective removal of emerging contaminants from water and wastewater. Env Pollut. 2021;280:116995.
[24] Sridharan R, Peter JD, Senthil Kumar P, Krishnaswamy VG. Acetaminophen degradation using bacterial strains isolated from winogradsky column and phytotoxicity analysis of dump site soil. Chemosphere. 2022;286(P1):131570.
[25] Liao G, Qing X, Xu P, Li L, Lu P, Chen W, et al. Synthesis of single atom cobalt dispersed on 2D carbon nanoplate and degradation of acetaminophen by peroxymonosulfate activation. Chem Eng J. 2022;427:132027.
[26] Kumari S, Kumar RN. River water treatment using electrocoagulation for removal of acetaminophen and natural organic matter. Chemosphere. 2021;273:128571.
[27] Lee WJ, Goh PS, Lau WJ, Ismail AF. Removal of pharmaceutical contaminants from aqueous medium: a state-of-the-art review based on paracetamol. Arab J Sci Eng. 2020;45(9):7109–35.
[28] Ma J, Ding Y, Chi L, Yang X, Zhong Y, Wang Z, et al. Degradation of benzotriazole by sulfate radical-based advanced oxidation process. Env Technol (U Kingd). 2021;42(2):238–47.
[29] Chanikya P, Nidheesh PV, Syam Babu D, Gopinath A, Suresh Kumar M. Treatment of dyeing wastewater by combined sulfate radical based electrochemical advanced oxidation and electrocoagulation processes. Sep Purif Technol. 2021;254:117570.
[30] Asgari E, Sheikhmohammadi A, Nourmoradi H, Nazari S, Aghanaghad M. Degradation of ciprofloxacin by photocatalytic ozonation process under irradiation with UVA: comparative study, performance and mechanism. Process Saf Env Prot. 2021;147:356–66.
[31] Hu CY, Kuan WH, Lee IJ, Liu YJ. PH-Dependent mechanisms and kinetics of the removal of acetaminophen by manganese dioxide. J Env Chem Eng. 2021;9(2):105129.
[32] Duan X, Sun H, Shao Z, Wang S. Nonradical reactions in environmental remediation processes: uncertainty and challenges. Appl Catal B Env. 2018;224:973–82.
[33] Kohantorabi M, Gholami MRM. XNi100-X (M = Ag, and Co) nanoparticles supported on CeO_2 nanorods derived from Ce-metal organic frameworks as an effective catalyst for reduction of organic pollutants: Langmuir–Hinshelwood kinetics and mechanism. N J Chem. 2017;41(19):10948–58.
[34] Xu Y, Shi X, Hua R, Zhang R, Yao Y, Zhao B, et al. Remarkably catalytic activity in reduction of 4-nitrophenol and methylene blue by Fe_3O_4@COF supported noble metal nanoparticles. Appl Catal B Env. 2020;260:118142.
[35] Moctezuma E, Leyva E, Palestino G, de Lasa H. Photocatalytic degradation of methyl parathion: reaction pathways and intermediate reaction products. J Photochem Photobiol A Chem. 2007;186(1):71–84.
[36] Blanco-Vega MP, Guzmán-Mar JL, Villanueva-Rodríguez M, Maya-Treviño L, Garza-Tovar LL, Hernández-Ramírez A, et al. Photocatalytic elimination of bisphenol A under visible light using Ni-doped TiO_2 synthesized by microwave assisted sol-gel method. Mater Sci Semicond Process. 2017;71:275–82.
[37] Pawelec B, Fierro JLG. Microwave-assisted synthesis of (S) Fe/TiO_2 systems: effects of synthesis conditions and dopant concentration on photoactivity. Appl Catal B: Environ. 2013;141:213–24.
[38] Kohantorabi M, Moussavi G, Mohammadi S, Oulego P, Giannakis S. Photocatalytic activation of peroxymonosulfate (PMS) by novel mesoporous Ag/ZnO@$NiFe_2O_4$ nanorods, inducing radical-mediated acetaminophen degradation under UVA irradiation. Chemosphere. 2021;277:130271.
[39] Hassani A, Eghbali P, Kakavandi B, Lin KYA, Ghanbari F. Acetaminophen removal from aqueous solutions through peroxymonosulfate activation by $CoFe_2O_4$/mpg-C_3N_4 nanocomposite: insight into the performance and degradation kinetics. Env Technol In. nov. 2020;20:101127.
[40] Da Silva WL, Lansarin MA, Dos Santos JHZ, Silveira F. Photocatalytic degradation of rhodamine B, paracetamol and diclofenac sodium by supported titania-based catalysts from petrochemical residue: effect of doping with magnesium. Water Sci Technol. 2016;74(10):2370–83.
[41] Ling Y, Liao G, Xu P, Li L. Fast mineralization of acetaminophen by highly dispersed Ag-*g*-C_3N_4 hybrid assisted photocatalytic ozonation. Sep Purif Technol. 2019;216:1–8.
[42] Hernández R, Olvera-Rodríguez I, Guzmán C, Medel A, Escobar-Alarcón L, Brillas E, et al. Microwave-assisted sol-gel synthesis of an Au-TiO_2 photoanode for the advanced oxidation of paracetamol as model pharmaceutical pollutant. Electrochem commun. 2018;96:42–6.
[43] Aziz FFA, Jalil AA, Triwahyono S, Mohamed M. Controllable structure of fibrous SiO_2 –ZSM-5 support decorated with TiO_2 catalysts for enhanced photodegradation of paracetamol. Appl Surf Sci. 2018;455:84–95.
[44] Yang L, Yu LE, Ray MB. Degradation of paracetamol in aqueous solutions by TiO_2 photocatalysis. Water Res. 2008;42(13):3480–8.
[45] Montenegro-Ayo R, Morales-Gomero JC, Alarcon H, Cotillas S, Westerhoff P, Garcia-Segura S. Scaling up photoelectrocatalytic reactors: a TiO_2 nanotube-coated disc compound reactor effectively degrades acetaminophen. Water (Switz). 2019;11(12):1–14.
[46] Sun P, Liu H, Feng M, Zhang X, Fang Y, Zhai Z, et al. Dual nonradical degradation of acetaminophen by peroxymonosulfate activation with highly reusable and efficient N/S co-doped ordered mesoporous carbon. Sep Purif Technol. 2021;268:118697.
[47] Wang X, Brigante M, Dong W, Wu Z, Mailhot G. Degradation of Acetaminophen via UVA-induced advanced oxidation processes (AOPs). Involvement of different radical species: $HO^{\cdot}$, $SO_4^{\cdot-}$ and $HO_2^{\cdot}/O_2^{\cdot-}$. Chemosphere. 2020;258:127268.
[48] Lin CJ, Yang WT. Ordered mesostructured Cu-doped TiO_2 spheres as active visible-light-driven photocatalysts for degradation of paracetamol. Chem Eng J. 2013;237:131–7.
[49] Feng X, Wang P, Hou J, Qian J, Wang C, Ao Y. Oxygen vacancies and phosphorus codoped black titania coated carbon nanotube composite photocatalyst with efficient photocatalytic performance for the degradation of acetaminophen under visible light irradiation. Chem Eng J. 2018;352:947–56.
[50] Ikhlaq A, Waheed S, Joya KS, Kazmi M. Catalytic ozonation of paracetamol on zeolite A: non-radical mechanism. Catal Commun. 2018;112:15–20.

[51] Do QC, Kim DG, Ko SO. Catalytic activity enhancement of a Fe_3O_4@SiO_2 yolk-shell structure for oxidative degradation of acetaminophen by decoration with copper. J Clean Prod. 2018;172:1243–53.
[52] Zhang Y, Zhang Q, Hong J. Sulfate radical degradation of acetaminophen by novel iron–copper bimetallic oxidation catalyzed by persulfate: mechanism and degradation pathways. Appl Surf Sci. 2017;422:443–51.
[53] Tan C, Gao N, Deng Y, Deng J, Zhou S, Li J, et al. Radical induced degradation of acetaminophen with Fe_3O_4 magnetic nanoparticles as heterogeneous activator of peroxymonosulfate. J Hazard Mater. 2014;276:452–60.
[54] Tan C, Gao N, Zhou S, Xiao Y, Zhuang Z. Kinetic study of acetaminophen degradation by UV-based advanced oxidation processes. Chem Eng J. 2014;253:229–36.
[55] Kurniawan TA, Yanyan L, Ouyang T, Albadarin AB, Walker G. $BaTiO_3$/TiO_2 composite-assisted photocatalytic degradation for removal of acetaminophen from synthetic wastewater under UV–vis irradiation. Mater Sci Semicond Process. 2018;73:42–50.
[56] Yaghmaeian K, Moussavi G, Mashayekh-Salehi A, Mohseni-Bandpei A, Satari M. Oxidation of acetaminophen in the ozonation process catalyzed with modified MgO nanoparticles: effect of operational variables and cytotoxicity assessment. Process Saf Env Prot. 2017;109:520–8.
[57] Fan G, Zheng X, Luo J, Peng H, Lin H, Bao M, et al. Rapid synthesis of Ag/AgCl@ZIF-8 as a highly efficient photocatalyst for degradation of acetaminophen under visible light. Chem Eng J. 2018;351:782–90.
[58] Tan C, Gao N, Fu D, Deng J, Deng L. Efficient degradation of paracetamol with nanoscaled magnetic $CoFe_2O_4$ and $MnFe_2O_4$ as a heterogeneous catalyst of peroxymonosulfate. Sep Purif Technol. 2017;175:47–57.
[59] Cheshme Khavar AH, Moussavi G, Mahjoub AR. The preparation of TiO_2@rGO nanocomposite efficiently activated with UVA/LED and H_2O_2 for high rate oxidation of acetaminophen: catalyst characterization and acetaminophen degradation and mineralization. Appl Surf Sci. 2018;440:963–73.
[60] Abdel-Wahab AM, Al-Shirbini AS, Mohamed O, Nasr O. Photocatalytic degradation of paracetamol over magnetic flower-like TiO_2/Fe_2O_3 core–shell nanostructures. J Photochem Photobiol A Chem. 2017;347:186–98.
[61] Lin CJ, Yang WT, Chou CY, Liou SYH. Hollow mesoporous TiO_2 microspheres for enhanced photocatalytic degradation of acetaminophen in water. Chemosphere. 2016;152:490–5.
[62] Bernal V, Erto A, Giraldo L, Moreno-Piraján JC. Effect of solution pH on the adsorption of paracetamol on chemically modified activated carbons. Molecules. 2017;22(7):1–14.
[63] Zhang Y, Zhang Q, Dong Z, Liying W, Hong J. Degradation of acetaminophen with ferrous/copperoxide activate persulfate: synergism of iron and copper. Water Res. 2018;146:232–43.
[64] Peng S, Feng Y, Liu Y, Wu D. Applicability study on the degradation of acetaminophen via an H_2O_2/PDS-based advanced oxidation process using pyrite. Chemosphere. 2018;212:438–46.
[65] Dong Z, Zhang Q, Hong J, Chen BY, Xu Q. Deciphering acetaminophen degradation using novel microporous beads reactor activate persulfate process with minimum iron leachate for sustainable treatment. Catal Lett. 2018;148(7):2095–108.
[66] Zhang Q, Huang W, Hong JM, Chen BY. Deciphering acetaminophen electrical catalytic degradation using single-form S doped graphene/Pt/TiO_2. Chem Eng J. 2018;343:662–75.
[67] Zhao L, Chen Y, Feng Y, Wu D. Oxidation of acetaminophen by Green rust coupled with Cu(II) via dioxygen activation: the role of various interlayer anions (CO_3^{2-}, SO_4^{2-}, Cl^-). Chem Eng J. 2018;350:930–8.
[68] Thi VHT, Lee BK. Effective photocatalytic degradation of paracetamol using La-doped ZnO photocatalyst under visible light irradiation. Mater Res Bull. 2017;96:171–82.
[69] Aziz FFA, Jalil AA, Hitam CNC, Hassan NS, Rahman AFA, Fauzi AA. Tailoring amount of TiO_2 doped onto fibrous silica ZSM-5 for enhanced photodegradation of paracetamol. IOP Conf Ser Mater Sci Eng. 2020;808(1):012017.
[70] Velichkova F, Julcour-Lebigue C, Koumanova B, Delmas H. Heterogeneous Fenton oxidation of paracetamol using iron oxide (nano) particles. J Env Chem Eng. 2013;1(4):1214–22.
[71] Zhang Y, Fan J, Yang B, Ma L. Synergistic effect of ferrous ion and copper oxide on the oxidative degradation of aqueous acetaminophen at acid conditions: a mechanism investigation. Chem Eng J. 2017;326:612–9.
[72] Im JK, Heo J, Boateng LK, Her N, Flora JRV, Yoon J, et al. Ultrasonic degradation of acetaminophen and naproxen in the presence of single-walled carbon nanotubes. J Hazard Mater. 2013;254–255(1):284–92.
[73] Soltani RDC, Miraftabi Z, Mahmoudi M, Jorfi S, Boczkaj G, Khataee A. Stone cutting industry waste-supported zinc oxide nanostructures for ultrasonic assisted decomposition of an anti-inflammatory non-steroidal pharmaceutical compound. Ultrason Sonochem. 2019;58:104669.
[74] Pham VL, Kim DG, Ko SO. Catalytic degradation of acetaminophen by Fe and N Co-doped multi-walled carbon nanotubes. Env Res. 2021;201:111535.
[75] Czech B, Tyszczuk-Rotko K. Visible-light-driven photocatalytic removal of acetaminophen from water using a novel MWCNT-TiO_2-SiO_2 photocatalysts. Sep Purif Technol. 2018;206:343–55.
[76] Chen Y, Zhang X, Mao L, Yang Z. Dependence of kinetics and pathway of acetaminophen photocatalytic degradation on irradiation photon energy and TiO_2 crystalline. Chem Eng J. 2017;330:1091–9.
[77] Radjenović J, Sirtori C, Petrović M, Barceló D, Malato S. Solar photocatalytic degradation of persistent pharmaceuticals at pilot-scale: kinetics and characterization of major intermediate products. Appl Catal B Env. 2009;89(1–2):255–64.
[78] Katal R, Tanhaei M, Hu J. Photocatalytic degradation of the acetaminophen by nanocrystal-engineered TiO_2 thin film in batch and continuous system. Front Env Sci Eng. 2021;15:21–4.
[79] Fernández Acosta R, Peláe Abellán E, Correa JR, Jáuregui Haza U. Nanostructured TiO_2 Obtained by Electrolysis and its Application in the Remediation of Water Polluted with Paracetamol. Int J Chem Mater Env Res. 2016;3(2):20–8.
[80] Hurtado L, Romero R, Mendoza A, Brewer S, Donkor K, Gómez-Espinosa RM, et al. Paracetamol mineralization by Photo Fenton process catalyzed by a Cu/Fe-PILC under circumneutral pH conditions. J Photochem Photobiol A Chem. 2019;373:162–70.

[81] Khani Z, Schieppati D, Bianchi CL, Boffito DC. The sonophotocatalytic degradation of pharmaceuticals in water by Mnox-TiO_2 systems with tuned band-gaps. Catalysts. 2019;9(11):1–20.
[82] Ghanbari F, Giannakis S, Lin KYA, Wu J, Madihi-Bidgoli S. Acetaminophen degradation by a synergistic peracetic acid/UVC-LED/Fe(II) advanced oxidation process: kinetic assessment, process feasibility and mechanistic considerations. Chemosphere. 2021;263:128119.
[83] Rad LR, Haririan I, Divsar F. Comparison of adsorption and photo-Fenton processes for phenol and paracetamol removing from aqueous solutions: single and binary systems. Spectrochim Acta – Part A Mol Biomol Spectrosc. 2015;136(PB):423–8.
[84] Audino F, Conte LO, Schenone AV, Pérez-Moya M, Graells M, Alfano OM. A kinetic study for the Fenton and photo-Fenton paracetamol degradation in an annular photoreactor. Env Sci Pollut Res. 2019;26(5):4312–23.
[85] Noorisepehr M, Ghadirinejad K, Kakavandi B, Ramazanpour Esfahani A, Asadi A. Photo-assisted catalytic degradation of acetaminophen using peroxymonosulfate decomposed by magnetic carbon heterojunction catalyst. Chemosphere. 2019;232:140–51.
[86] Palas B, Ersöz G, Atalay S. Bioinspired metal oxide particles as efficient wet air oxidation and photocatalytic oxidation catalysts for the degradation of acetaminophen in aqueous phase. Ecotoxicol Env Saf. 2019;182:109367.
[87] Behravesh S, Mirghaffari N, Alemrajabi AA, Davar F, Soleimani M. Photocatalytic degradation of acetaminophen and codeine medicines using a novel zeolite-supported TiO_2 and ZnO under UV and sunlight irradiation. Env Sci Pollut Res. 2020;27(21):26929–42.
[88] Yanyan L, Kurniawan TA, Ying Z, Albadarin AB, Walker G. Enhanced photocatalytic degradation of acetaminophen from wastewater using $WO_3/TiO_2/SiO_2$ composite under UV–VIS irradiation. J Mol Liq. 2017;243:761–70.
[89] Santos-Juanes L, García Einschlag FS, Amat AM, Arques A. Combining ZVI reduction with photo-Fenton process for the removal of persistent pollutants. Chem Eng J. 2017;310:484–90.
[90] Farhadi ARK, Rahemi N, Allahyari S, Tasbihi M. Metal-doped perovskite $BiFeO_3$/rGO nanocomposites towards the degradation of acetaminophen in aqueous phase using plasma-photocatalytic hybrid technology. J Taiwan Inst Chem Eng. 2021;120:77–92.
[91] Lin JCTe, de Luna MDG, Aranzamendez GL, Lu MC. Degradations of acetaminophen via a $K_2S_2O_8$-doped TiO_2 photocatalyst under visible light irradiation. Chemosphere. 2016;155:388–94.
[92] Trovó AG, Pupo Nogueira RF, Agüera A, Fernandez-Alba AR, Malato S. Paracetamol degradation intermediates and toxicity during photo-Fenton treatment using different iron species. Water Res. 2012;46(16):5374–80.
[93] Xiao X, Hu R, Liu C, Xing C, Qian C, Zuo X, et al. Facile large-scale synthesis of β-Bi_2O_3 nanospheres as a highly efficient photocatalyst for the degradation of acetaminophen under visible light irradiation. Appl Catal B Env. 2013;140–141:433–43.
[94] Hinojosa Guerra MM, Oller Alberola I, Malato Rodriguez S, Agüera López A, Acevedo Merino A, Egea-Corbacho Lopera A, et al. Oxidation mechanisms of amoxicillin and paracetamol in the photo-Fenton solar process. Water Res. 2019;156:232–40.
[95] Darvishi-Farash S, Afsharpour M, Heidarian J. Novel siligraphene/g-C_3N_4 composites with enhanced visible light photocatalytic degradations of dyes and drugs. Env Sci Pollut Res. 2021;28(5):5938–52.
[96] Wang YL, Zhang S, Zhao YF, Bedia J, Rodriguez JJ, Belver C. UiO-66-based metal organic frameworks for the photodegradation of acetaminophen under simulated solar irradiation. J Env Chem Eng. 2021;9(5):106087.
[97] Khasawneh OFS, Palaniandy P, Palaniandy P, Ahmadipour M, Bin Mohammadi H, Hamdan MR. Removal of acetaminophen using Fe_2O_3–TiO_2 nanocomposites by photocatalysis under simulated solar irradiation: optimization study. J Env Chem Eng. 2021;9(1):104921.
[98] Pires J, Borges S, Carvalho A, Pereira C, Pereira AM, Fernandes C, et al. Magnetically recyclable mesoporous iron oxide-silica materials for the degradation of acetaminophen in water under mild conditions. Polyhedron. 2016;106:125–31.
[99] Im JK, Yoon J, Her N, Han J, Zoh KD, Yoon Y. Sonocatalytic-TiO_2 nanotube, Fenton, and CCl_4 reactions for enhanced oxidation, and their applications to acetaminophen and naproxen degradation. Sep Purif Technol. 2015;141:1–9.
[100] Augusto TDM, Chagas P, Sangiorge DL, Mac Leod TCDO, Oliveira LCA, Castro CSDe. Iron ore tailings as catalysts for oxidation of the drug paracetamol and dyes by heterogeneous Fenton. J Env Chem Eng. 2018;6(5):6545–53.
[101] Zhang H, Cao B, Liu W, Lin K, Feng J. Oxidative removal of acetaminophen using zero valent aluminum-acid system: efficacy, influencing factors, and reaction mechanism. J Env Sci. 2012;24(2):314–9.
[102] Jiang M, Lu J, Ji Y, Kong D. Bicarbonate-activated persulfate oxidation of acetaminophen. Water Res. 2017;116:324–31.
[103] de Luna MDG, Briones RM, Su CC, Lu MC. Kinetics of acetaminophen degradation by Fenton oxidation in a fluidized-bed reactor. Chemosphere. 2013;90(4):1444–8.
[104] Slamani S, Abdelmalek F, Ghezzar MR, Addou A. Initiation of Fenton process by plasma gliding arc discharge for the degradation of paracetamol in water. J Photochem Photobiol A Chem. 2018;359:1–10.
[105] Su CC, Bellotindos LM, Chang AT, Lu MC. Degradation of acetaminophen in an aerated Fenton reactor. J Taiwan Inst Chem Eng. 2013;44(2):310–6.
[106] Pham VL, Kim DG, Ko SO. Advanced oxidative degradation of acetaminophen by carbon catalysts: radical vs non-radical pathways. Env Res. 2020;188:109767.
[107] Tan C, Sheng T, Xu Q, Xu T, Sun K, Deng L, et al. Cobalt doped iron oxychloride as efficient heterogeneous Fenton catalyst for degradation of paracetamol and phenacetin. Chemosphere. 2021;263:127989.
[108] Palas B, Ersöz G, Atalay S. Biotemplated copper oxide catalysts over graphene oxide for acetaminophen removal: reaction kinetics analysis and cost estimation. Chem Eng Sci. 2021;242:116593.
[109] Benzaquén TB, Ochoa Rodriguez PA, Cánepa AL, Casuscelli SG, Elías VR, Eimer GA. Heterogeneous Fenton reaction for the treatment of ACE in residual waters of

pharmacological origin using Fe-SBA-15 nanocomposites. Mol Catal. 2020;481:110239.
[110] Shi Y, Zhang Y, Cui Y, Shi J, Meng X, Zhang J, et al. Magnetite nanoparticles modified β-cyclodextrin PolymerCoupled with $KMnO_4$ oxidation for adsorption and degradation of acetaminophen. Carbohydr Polym. 2019;222:114972.
[111] Fan J, Qin H, Jiang S. Mn-doped g-C_3N_4 composite to activate peroxymonosulfate for acetaminophen degradation: the role of superoxide anion and singlet oxygen. Chem Eng J. 2019;359:723–32.
[112] Zhang G, Sun Y, Zhang C, Yu Z. Decomposition of acetaminophen in water by a gas phase dielectric barrier discharge plasma combined with TiO_2-rGO nanocomposite: mechanism and degradation pathway. J Hazard Mater. 2017;323:719–29.
[113] Zhang Y, Fan J, Yang B, Huang W, Ma L. Copper–catalyzed activation of molecular oxygen for oxidative destruction of acetaminophen: the mechanism and superoxide-mediated cycling of copper species. Chemosphere. 2017;166:89–95.
[114] Zhu J, Zhu Z, Zhang H, Lu H, Qiu Y. Calcined CoAl-layered double hydroxide as a heterogeneous catalyst for the degradation of acetaminophen and rhodamine B: activity, stability, and mechanism. Env Sci Pollut Res. 2019;26(32):33329–40.
[115] Rashidashmagh F, Doekhi-Bennani Y, Tizghadam-Ghazani M, van der Hoek JP, Mashayekh-Salehi A, Heijman BSGJ, et al. Synthesis and characterization of SnO2 crystalline nanoparticles: a new approach for enhancing the catalytic ozonation of acetaminophen. J Hazard Mater. 2021;404:124154.
[116] Hachemaoui M, Molina CB, Belver C, Bedia J, Mokhtar A, Hamacha R, et al. Metal-loaded mesoporous mcm-41 for the catalytic wet peroxide oxidation (CWPO) of acetaminophen. Catalysts. 2021;11(2):1–17.
[117] Tan W, Ma Y, Ren W, Fan Y, Liu X, Xu Y, et al. Removal of acetaminophen through direct electron transfer by reactive Mn_2O_3: efficiency, mechanism and pathway. Sci Total Env. 2021;769:144377.
[118] Do QC, Kim DG, Ko SO. Nonsacrificial template synthesis of magnetic-based yolk-shell nanostructures for the removal of acetaminophen in fenton-like systems. ACS Appl Mater Interfaces. 2017;9(34):28508–18.